Speleothem records from western Thailand indicate an early rapid shift of the Indian summer monsoon during the Younger Dryas termination

Matthew J. Jacobson [a,*], Sakonvan Chawchai [b,**], Denis Scholz [c], Dana F.C. Riechelmann [c], Karin Holmgren [a], Hubert Vonhof [d], Xianfeng Wang [e], Guangxin Liu [f]

[a] *Division of Agrarian History, Department of Urban and Rural Development, Swedish University of Agricultural Sciences, Uppsala, 756 51, Sweden*
[b] *Past and Present Climate Towards the Future Research Unit (PPCTF), Department of Geology, Faculty of Science, Chulalongkorn University, Bangkok, 10330, Thailand*
[c] *Institute for Geosciences, Johannes Gutenberg University Mainz, Mainz, 55128, Germany*
[d] *Climate Geochemistry Department, Max Planck Institute for Chemistry, Mainz, 55128, Germany*
[e] *Earth Observatory of Singapore & Asian School of the Environment, Nanyang Technological University, 636798, Singapore*
[f] *Yunnan Key Laboratory of Meteorological Disasters and Climate Resources in the Greater Mekong Subregion, Yunnan University, Kunming, 650091, China*

ARTICLE INFO

ABSTRACT

Mainland Southeast Asia experiences complex and variable hydroclimatic conditions, mainly due to its location at the intersection of Asian monsoon subsystems. Predicting future changes requires an in-depth understanding of paleoclimatic conditions that is currently hindered by a paucity of records in some regions. In this paper, we present the first speleothem stable isotope records from western Thailand detailing the Bølling-Allerød inter-stadial, Younger Dryas termination, and early- to mid-Holocene period. We find evidence of higher precipitation during the Bølling-Allerød (14,321–12,824 years before present (1950: BP)) compared to a Younger Dryas termination that starts 11,702–11,674 BP, has a rapid shift centered on 11,660–11,641 BP, and ends 11,603–11,589 BP. In addition, our records show Holocene monsoon intensity peaking at 8250 BP or before, a multi-millennia delay from the Northern Hemisphere summer insolation peak, followed by a trend to drier conditions until at least 750 BP. Assessment of the timing of the Younger Dryas termination in paleoclimate records across Southeast Asia reveals an earlier shift of the Indian Summer Monsoon to global climate shifts when compared to East Asian Summer Monsoon records. The causes of this are currently unknown. Some potentially important aspects include: an Indian Summer Monsoon influence on East Asian Summer Monsoon strength via the Indian Ocean Dipole climate pattern, the role of the Tibetan Plateau in monsoon dynamics, and exposure of the Sundaland shoreline. More high-resolution paleoclimate records, especially on the pathway of Indian Summer Monsoon to East Asian Summer Monsoon, are required for further discussion on the mechanisms controlling the differences between climate regimes.

1. Introduction

Hydroclimatic conditions in mainland Southeast Asia (SEA) are complex, with varying precipitation regimes resulting from topography, land-sea interactions, and most importantly, its location at the inter-section of the East Asian Winter Monsoon (EAWM) and the three Asian Summer Monsoon (ASM) systems: the Indian Summer Monsoon (ISM), Western North Pacific Summer Monsoon (WNPSM) and the East Asian Summer Monsoon (EASM) (Wang and LinHo, 2002). In Thailand, these conditions result in a characteristic precipitation pattern of summer

(JJAS) monsoon and winter (NDJFM) dry seasons. However, being in the monsoon intersection zone, on the path of the seasonal migration of the Intertropical Convergence Zone (ITCZ) and close to the boundaries of varied precipitation regimes, means the seasonality of precipitation across mainland SEA changed in the past and likely will again in the future (Chawchai et al., 2015; Kuang et al., 2021; Lan et al., 2023; Yuan et al., 2023). Adding to this complexity, sea level substantially changed since the Last Glacial Maximum (21,000 years before present (1950: BP hereafter)), when it was ~120 m below current levels and a large amount of landmass ("Sundaland") was exposed. Subsequently, it

gradually rose to a highstand of ~3–5 m asl. Between 7000 and 5000 BP and then fell to present levels (Leknettip et al., 2023; Sathiamurthy and Voris, 2006; Surakiatchai et al., 2018). Changes in land exposure influenced precipitation regimes via altered rainout and land-sea thermal contrasts (Bird et al., 2005; Chabangborn et al., 2014; De Deckker et al., 2003). Furthermore, aspects of the global climate system have impacted the region, such as meltwater in the North Atlantic weakening Atlantic Meridional Overturning Circulation (AMOC) and altering monsoon variability via the ITCZ during glacial terminations (Wassenburg et al., 2021; Yuan et al., 2023).

Climatic fluctuations can have significant impacts on people in mainland SEA due to high population density, with a reliance on agriculture that requires predictable monsoon rains (Pereira and Shaw, 2022). Constraining past climatic variability is crucial for future climate predictions and successful mitigation strategies; however, this remains a significant challenge in SEA due to the shifting monsoons, teleconnections, external forcings and physical geography outlined above. One still poorly understood aspect is the specific regional responses to global abrupt change/events, for instance the termination of the Younger Dryas (YD), the shift from a cold glacial world to the warmer interglacial state of the Holocene. In Thailand, researchers have extensively studied tree-rings for paleoclimate reconstructions, producing highly resolved and well-dated records of precipitation, river flow, and monsoon variability (e.g., Xu et al., 2019; Nguyen et al., 2022; Preechamart et al., 2023). Whilst invaluable for understanding recent climate change and dynamics, tree-ring records unfortunately only extend back centuries and the necessity to remove the age-related growth trend in tree-ring widths can result in the erasure of longer-term trends (Büntgen, 2022). To resolve SEA climate changes in earlier periods, paleoclimatologists utilize records produced from lake sediments (e.g., Chawchai et al., 2015; Hamilton et al., 2019; Yamoah et al., 2021) and speleothems (i.e., stalagmites) (e.g., Wang et al., 2019; Chawchai et al., 2021; Buckingham et al., 2022). However, in mainland SEA, coverage of these records is spatio-temporally incomplete (Fig. 1). This is especially true for the monsoon intersection zone in mainland SEA, where the requirement for more data has long been noted (Hamilton et al., 2019; Wohlfarth et al., 2012). Whilst there are several published records from the region, most only detail conditions later in the Holocene (Khao Prae, Klang, Kumphawapi, Lin Noe Twin, Pa Kho, Thien Duong, Tonle Sap, Yeak Mai) and/or much earlier (Lin Noe Twin, Pa Kho) (Chawchai et al., 2013, 2015, 2020, 2021; Hamilton et al., 2019; Liu et al., 2020; Penny, 2006; Wolf et al., 2023; Yamoah et al., 2016, 2021). In fact, there is currently only one record detailing conditions during the YD termination: the Hoa Huong Cave $\delta^{18}O$ record from Central Vietnam, which pertains to autumn/winter monsoon intensity in the period 45,000–4000 BP (Patterson et al., 2023). As no records detail ASM variability in the monsoon intersection zone at the late Pleistocene-Holocene transition, producing some is critical for developing a greater understanding of regional responses.

Usually in glacial terminations, increasing temperatures cause a release of iceberg material and meltwater in the North Atlantic, strengthening the AMOC and ASM (Clark et al., 2012; Sandeep et al., 2020; Sun et al., 2012; Wassenburg et al., 2021). However, the timing of the YD termination, which is evidenced earlier in the Southern Hemisphere and western tropical pacific when compared to monsoonal Asia and the North Atlantic (Cheng et al., 2020), does not allow for a North Atlantic origin. Despite the value of establishing differential timing of the YD termination globally for understanding its propagation and causes (e.g., Cheng et al., 2020), more could be done to examine the timing variability across smaller spatial scales.

To reconcile differences in the timing of the YD termination between regions, we present two new speleothem oxygen ($\delta^{18}O$) and carbon ($\delta^{13}C$) stable isotope records (TKD-1 and TKD-2) from Tham Khao Dang Cave, western Thailand, which extend back to 14,500 BP. These records are the first from western mainland SEA covering the Bølling–Allerød (BA) interstadial (TKD-2) and the first from western Thailand detailing
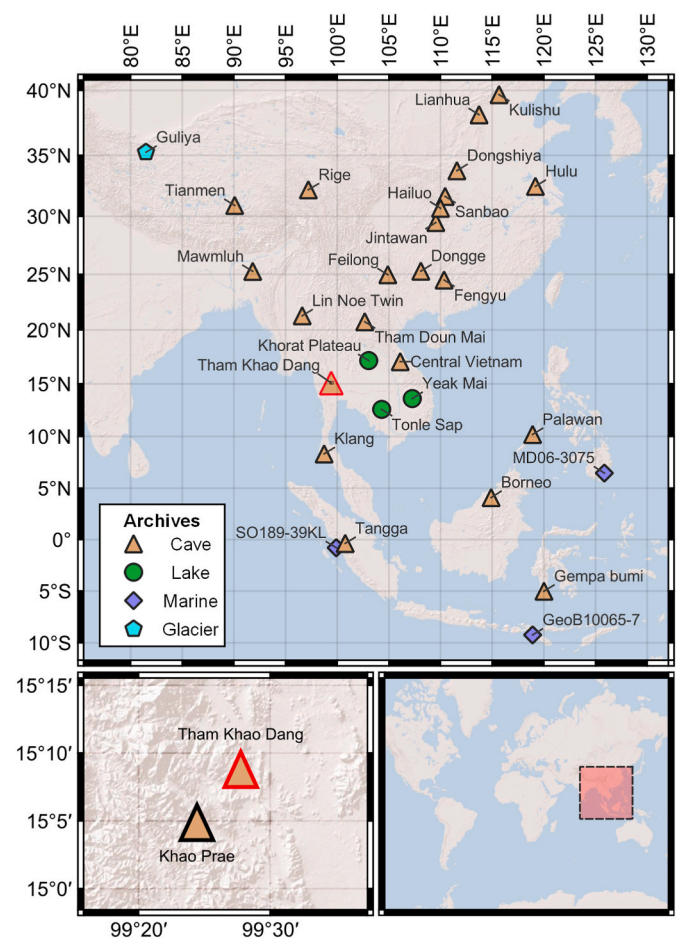

Fig. 1. Maps showing the locations of paleoclimate records discussed in this study alongside Tham Khao Dang (highlighted red). Proximate archives of the same type are grouped for clarity and labelled: Khorat Plateau (Kumphawapi and Pa Kho), Central Vietnam (Hoa Huong and Thien Duong), and Borneo (Gunung Mulu, Bukit Assam and Gunung-buda). Bottom left panel shows Ban Rai District and the proximity of Tham Khao Dang to Khao Prae Cave (Chawchai et al., 2020). Bottom right panel locates Southeast Asia globally.

the YD termination (TKD-1 and TKD-2) and Mid Holocene (TKD-1). With these new records, we identify trends in the climatic evolution of western Thailand in the Late Pleistocene-Holocene period. Principally, we establish a chronology for the termination of the YD and determine long-term trends during the Holocene. Further, we perform Bayesian Change Point Analysis (BCP) on select paleoclimate records to examine the timing variability of the YD termination, we discuss the variation of these patterns between regions, and explore the mechanisms behind its differences and propagation.

2. Climatic and environmental settings

Tham Khao Dang (TKD) Cave (15°08′ N, 99°27′ E; ~400 m asl) is located in Ban Rai district, southern Uthai Thani province, western Thailand (Fig. 1), and is formed within argillaceous limestone of Ordovician age (Chawchai et al., 2018). The inner chambers of the cave, where stalagmite samples were collected from, were well enclosed and during two separate fieldwork visits (2015 and 2017) had a steady cave temperature of 23–24 °C and humidity of 91–92 %. It is located less than 8 km north of the previously-studied Khao Prae Cave (Chawchai et al., 2020) and approximately 170 km from the Andaman Sea coast. At both caves, bamboo and teak (*Tectona grandis*) form a dense mixed deciduous forest, which is typical for western Thailand (Marod et al., 1999). The loamy soil above the cave has a thickness of around 1 m. Today, TKD

Cave is quite dry, has only one entrance and contains several small chambers.

According to the CRU TS4.06 (1901–2021), the average annual temperature and precipitation sum outside the cave are 24.8 °C and 1750 mm, respectively (University of East Anglia Climatic Research Unit et al., 2022). On average, there are 105 rainy days per year (Chawchai et al., 2018). Conditions are dry between November and March, averaging 4–42 mm and rarely exceeding 100 mm per month. Precipitation is more varied during the monsoon season (June–September), ranging between 120 and 500 mm per month (Fig. 2). On average, this accounts for 66 % of annual precipitation, but with a range from 47 % (1990) to 84 % (1930). The Köppen-Geiger climate classification of western Thailand, and most of mainland SEA, is "Tropical, savannah" (Aw), with smaller amounts of "Tropical, monsoon" (Am) (Beck et al., 2018). Monthly temperature exhibits a marked peak in April, at an average of 27.6 °C, alongside many extreme daily temperatures (e.g., on April 15, 2023, when a new maximum of 45.5 °C was reached).

3. Materials and methods

Two broken stalagmites (TKD-1 and TKD-2, Fig. 3) were collected separately from two chambers of Tham Khao Dang Cave in 2015. TKD-1 is approximately 21 cm long and 7 cm wide, and is comprised of two candle-shape sections with a distinct change in growth axis between them. TKD-2 is one single candle-shaped stalagmite, and 11 cm long and 6 cm wide.

3.1. Chronology

We drilled samples for ^{230}Th/U-dating as close to the growth axis as possible (Fig. 3). Dating was performed using Thermo Scientific Neptune Plus multicollector inductively coupled plasma mass spectrometers (MC-ICP-MS) at both the Institute for Geosciences, Johannes Gutenberg-University, Mainz, Germany, and the Earth Observatory of Singapore (EOS), Nanyang Technological University, Singapore, following the analytical protocol of Cheng et al. (2013). In Mainz, the weighed powder samples were dissolved in 7N HNO$_3$, and a mixed ^{229}Th–^{233}U–^{236}U spike was added (see Gibert et al., 2016, for details on spike calibration). Potential organic material was removed by adding a mixture of

Fig. 3. Speleothem scans with growth axes (black lines) and sampling locations for uranium-series ages (red ovals). Stars indicate ^{230}Th/U uranium-series ages repeated on the opposite "face" of the sample.

concentrated HNO$_3$, HCl and H$_2$O$_2$. Then, the samples were dried down and afterwards dissolved in 7N HNO$_3$. Uranium and Thorium were separated using ion exchange column chemistry (Yang et al., 2015). Details of the MC-ICP-MS procedures are described in Obert et al. (2016). In Singapore, we measured intensities of all uranium and thorium isotopes with a peak-jumping protocol on a secondary electron multiplier equipped with a retarding potential quadrupole lens to improve abundance sensitivity, except for the isotopes ^{238}U and ^{232}Th, which were measured on Faraday cups. All activity ratios were calculated using the decay constants of Cheng et al. (2013). To account for potential detrital contamination, all ages were corrected assuming an upper continental crust ^{232}Th/^{238}U weight ratio of 3.8 ± 1.9 (Wedepohl, 1995) and secular equilibrium between ^{230}Th, ^{234}U, and ^{238}U. We utilized the StalAge algorithm (Scholz and Hoffmann, 2011) to calculate the chronologies of TKD-1 and TKD-2 from a total of 14 and 11 uranium-series ages, respectively.

For regional synthesis and comparison with other paleoclimate records from SEA, age uncertainties discussed throughout the text are extracted from each records age model, except in cases where the full age model is not provided by the original authors. In such cases, the uncertainty of the closest absolute age is given; for the YD termination, whether uncertainties are based on the age model or absolute ages is outlined in Supplementary Table S1.

3.2. Stable isotope analysis

We sampled TKD-1 and TKD-2 for oxygen (δ^{18}O) and carbon (δ^{13}C) stable isotope measurements along the growth axes at a 1 mm resolution, resulting in 200 samples for TKD-1 and 113 samples for TKD-2 (Supplementary Table S2). We drilled both speleothems using a New Wave Research MicroMill (Dettman and Lohmann, 1995). The samples
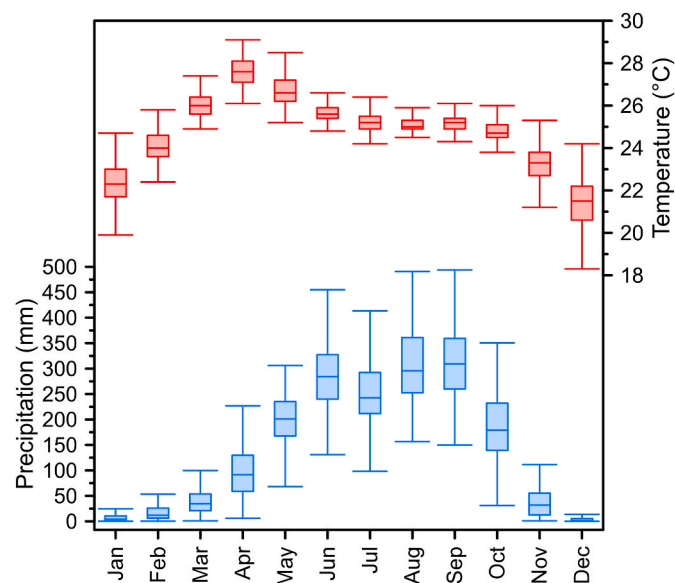

Fig. 2. Monthly temperature and precipitation averages (1901–2021) for Uthai Thani province (15–15.5° N, 99–99.5° E), from CRU TS4.06 (University of East Anglia Climatic Research Unit et al., 2022). Data were generated in the KNMI Climate Explorer (van Oldenborgh, 2020).

were analyzed with a Thermo Delta V continuous flow isotope ratio mass spectrometer equipped with a Gasbench II at the Max Planck Institute for Chemistry Mainz, Germany. Results are reported as per mil (‰) difference relative to the Vienna-Peedee Belemnite (VPDB) scale and are calibrated against the official reference material NBS19. The reproducibility of a routinely analyzed lab $CaCO_3$ reference material was better than 0.11‰ for both $\delta^{18}O$ and $\delta^{13}C$ values (1 standard deviation).

3.3. Bayesian Change Point Analysis (BCP)

Visually identifying the start, end, and most significant shift of the YD termination is challenging and suffers from inherent bias and human error. Therefore, we quantitatively assess these chronological differences on key records over the YD termination period (12,400–10,800 BP) with Bayesian Change Point Analysis (BCP) using the R Statistical Software (v4.3.0; R Core Team, 2023) and the package "bcp" (Erdman and Emerson, 2008; Wang and Emerson, 2015). This statistical package assesses segments of linear datasets to identify significant changes in their sample mean and variance, providing a probability of a change point occurring at every location in the sequence. We subsequently identify the highest probability change points in each record, using a threshold minimum probability of 0.7. BCP is preferable for our analysis as we largely focus on the timing of the most significant shift of the termination, which would not be identified with other statistical methods. Further, other methods that focus on trends, such as RAMPFIT and BREAKFIT (Mudelsee, 2000, 2009), have already been applied to many of the records discussed in this paper (e.g., see a comprehensive review in Cheng et al., 2020) and we compare to these previous results where necessary.

4. Results and interpretation

4.1. Chronology

The corrected $^{230}Th/U$-ages are all in stratigraphic order, and for TKD-1, the dates have uncertainties ranging from ±76–2395 years (average = ± 762). For TKD-2, uncertainties range from ±120–1900

years (average = ± 716). We summarize the results of uranium-series dating in Table 1, with all errors given at the 2σ-level (2 standard deviations). Almost all $^{230}Th/^{232}Th$ activity ratios range from 1.51 to 31.47, far lower than 200, suggesting a significant contribution of initial detrital ^{230}Th (Richards and Dorale, 2003), only one age shows more at 235.25. This is also evident from the differences between the uncorrected and corrected ages, which is in many cases larger than the analytical uncertainty. This is accounted for by the conservative assumed uncertainty of 50 % for the $^{232}Th/^{238}U$ weight ratio of the detritus and the corresponding error propagation, which results in substantially increased uncertainty for some of the corrected ages. Several hiatuses were discernible through examination of the $^{230}Th/U$-ages and visual analysis (macro- and micro-scopic) of the speleothems, which identified detrital layers. From the StalAge age-depth models (Fig. 4), it is clear that TKD-1 grew in five different phases, starting at 12,054 ± 86 BP whilst TKD-2 grew in three phases beginning at 14,321 ± 561 BP (see Table 2). Growth rates during different phases of TKD-1 varied from 8 to 67 μm/yr (average = 49 μm/yr), whilst for TKD-2, they varied from 34 to 61 μm/yr (average = 38 μm/yr). The resolution of the stable isotope records (see below) varied from 16 to 124 years between samples (average = 38 years) in TKD-1 and from 17 to 30 years between samples (average = 28 years per sample) in TKD-2 (Table 2).

4.2. Tham Khao Dang Cave stable-isotope records

Speleothem $\delta^{18}O$ values range from −11.5 ‰ to −6.9 ‰ (average = −9.6 ‰) in TKD-1 and -10.8 ‰ to −6.9 ‰ (average = −8.9 ‰) in TKD-2. TKD $\delta^{18}O$ records show relatively rapid decrease during the YD termination (11,675–11,630 BP) and a gradual increase over most of the Holocene (Fig. 5, full data in Supplementary Table S1). Speleothem $\delta^{18}O$ values have been widely applied as a proxy for monsoon intensity across the ASM region, largely determined by the $\delta^{18}O$ values of precipitation ($\delta^{18}O_p$) as influenced by the resulting precipitation amount (Chawchai et al., 2020; Lechleitner et al., 2017; Li et al., 2022; Wang et al., 2019). In these cases, lower (higher) $\delta^{18}O$ values reflect wetter (drier) conditions and a stronger (weaker) monsoon. In addition, a two-year time series of

Table 1

Results of $^{230}Th/U$-dating. All ages are reported as before the year 1950 CE(ka BP), and the errors are given at the 2σ-level. All activity ratios and $^{230}Th/U$-ages were calculated using the half-lives of Cheng et al. (2013). To account for potential detrital contamination, corrected ages were calculated assuming an upper continental crust $^{232}Th/^{238}U$ weight ratio of 3.8 ± 1.9 (Wedepohl, 1995) and secular equilibrium between ^{230}Th, ^{234}U, and ^{238}U. (dft: depth from top); * marks the samples dated in Singapore.

| Sample	dft [mm]	^{238}U [μg/g]	$(^{234/238}U)$	$(^{230/238}U)$	$(^{230/232}Th)$	Age uncorr. [ka BP]	Age corr. [ka BP]
TKD1a I	22	0.10930 ± 0.00067	1.08041 ± 0.00073	0.0226 ± 0.0019	5.393 ± 0.043	2.635 ± 0.021	2.24 ± 0.20
TKD1a II	59	0.08050 ± 0.00052	1.0810 ± 0.0017	0.061 ± 0.017	2.125 ± 0.016	9.891 ± 0.071	6.2 ± 1.8
TKD1b I	86	0.13169 ± 0.00081	1.0817 ± 0.0012	0.090 ± 0.011	3.736 ± 0.025	11.887 ± 0.072	9.4 ± 1.2
TKD1c I	135	0.10951 ± 0.00070	1.08098 ± 0.00075	0.1069 ± 0.0018	22.94 ± 0.16	11.675 ± 0.069	11.28 ± 0.21
TKD1-III	14	0.11398 ± 0.00070	1.08077 ± 0.00080	0.0144 ± 0.0049	1.968 ± 0.012	2.390 ± 0.015	1.39 ± 0.51
TKD1-IV	25	0.08079 ± 0.00050	1.08186 ± 0.00086	0.0285 ± 0.0029	4.699 ± 0.036	3.432 ± 0.026	2.84 ± 0.29
TKD1-V	49	0.09148 ± 0.00056	1.08032 ± 0.00066	0.03448 ± 0.00099	14.726 ± 0.093	3.671 ± 0.024	3.47 ± 0.10
TKD1-VI	75	0.01943 ± 0.00012	1.0834 ± 0.0024	0.073 ± 0.023	2.004 ± 0.013	12.399 ± 0.085	7.6 ± 2.4
TKD1a-t	59	0.10641 ± 0.00068	1.0818 ± 0.0012	0.048 ± 0.012	2.375 ± 0.016	7.295 ± 0.052	4.9 ± 1.2
TKD1a-b	75	0.06364 ± 0.00040	1.0828 ± 0.0014	0.067 ± 0.014	2.566 ± 0.016	9.931 ± 0.065	6.9 ± 1.5
TKD1b-t	91	0.11709 ± 0.00072	1.07537 ± 0.00050	0.0992 ± 0.0016	24.99 ± 0.12	10.800 ± 0.055	10.47 ± 0.17
TKD1b-b	115	0.11226 ± 0.00070	1.07622 ± 0.00059	0.1025 ± 0.0022	18.237 ± 0.078	11.308 ± 0.052	10.83 ± 0.24
TKD1-1-T*	0.1	0.2434 ± 0.0011	1.0777 ± 0.0031	0.01599 ± 0.00020	1.510 ± 0.036	1.564 ± 0.021	0.69 ± 0.62
TKD1-2-B*	196	0.11602 ± 0.00033	1.0784 ± 0.0021	0.11328 ± 0.00059	235.35 ± 5.58	12.020 ± 0.071	11.981 ± 0.076
TKD2 I	18	0.11010 ± 0.00068	1.0832 ± 0.0013	0.106 ± 0.012	3.993 ± 0.025	13.774 ± 0.078	11.1 ± 1.3
TKD2 II	55	0.12786 ± 0.00081	1.08039 ± 0.00081	0.1114 ± 0.0043	10.172 ± 0.080	12.762 ± 0.090	11.80 ± 0.49
TKD2 III	97	0.1553 ± 0.0010	1.07811 ± 0.00083	0.1276 ± 0.0071	7.205 ± 0.054	15.27 ± 0.10	13.66 ± 0.81
TKD2-IV	10	0.14241 ± 0.00089	1.08294 ± 0.00048	0.0104 ± 0.0011	4.481 ± 0.028	1.2103 ± 0.0080	0.98 ± 0.12
TKD2-V	62	0.11708 ± 0.00076	1.07991 ± 0.00060	0.1121 ± 0.0042	10.421 ± 0.039	12.822 ± 0.048	11.88 ± 0.47
TKD2-VI	67	0.11207 ± 0.00072	1.08425 ± 0.0017	0.124 ± 0.017	3.428 ± 0.016	16.913 ± 0.075	13.2 ± 1.9
TKD2-t	23	0.08663 ± 0.00056	1.08425 ± 0.00071	0.1033 ± 0.0013	31.47 ± 0.16	11.108 ± 0.060	10.84 ± 0.15
TKD2-m	72	0.1803 ± 0.0012	1.0795 ± 0.0012	0.122 ± 0.011	4.718 ± 0.015	15.535 ± 0.054	13.0 ± 1.3
TKD2-b	82	0.12566 ± 0.00084	1.07557 ± 0.00068	0.1275 ± 0.0044	11.008 ± 0.038	14.681 ± 0.056	13.67 ± 0.50
TKD-2-T*	5	0.11690 ± 0.00066	1.0818 ± 0.0042	0.01442 ± 0.00021	3.261 ± 0.081	1.397 ± 0.022	1.03 ± 0.26
TKD-2-B*	109	0.10223 ± 0.00030	1.0726 ± 0.0021	0.13964 ± 0.00076	14.24 ± 0.30	15.120 ± 0.094	14.31 ± 0.58
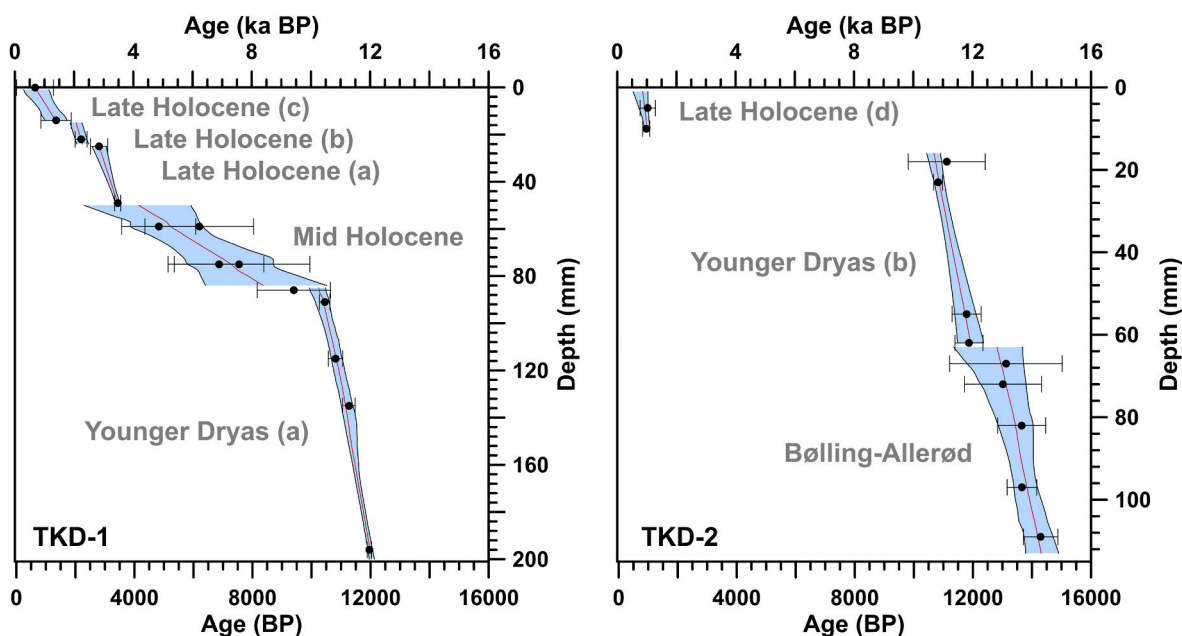
Fig. 4. Age-depth models of samples TKD-1 and TKD-2, calculated with StalAge (Scholz and Hoffmann, 2011). Blue shaded area represents the 95% confidence interval. Corresponding periods of growth phases (from Table 2) labelled in grey. ka BP corresponds to 1×10^3 BP.

Table 2
Growth phases of TKD speleothems, their corresponding periods, and characteristics.

| Growth Phase	Period Name	Sample	Start (BP)	End (BP)	Average Age Uncertainty (years)	Average Isotopic Resolution (years)
1	Bølling-Allerød	TKD-2	14,321	12,824	592	30
2	Younger Dryas (a)	TKD-1	12,054	10,260	148	16
3	Younger Dryas (b)	TKD-2	11,939	10,699	252	27
4	Mid Holocene	TKD-1	8389	4177	1408	124
5	Late Holocene (a)	TKD-1	3472	2843	137	26
6	Late Holocene (b)	TKD-1	2285	2065	201	25
7	Late Holocene (c)	TKD-1	1377	734	368	49
8	Late Holocene (d)	TKD-2	1017	864	156	17
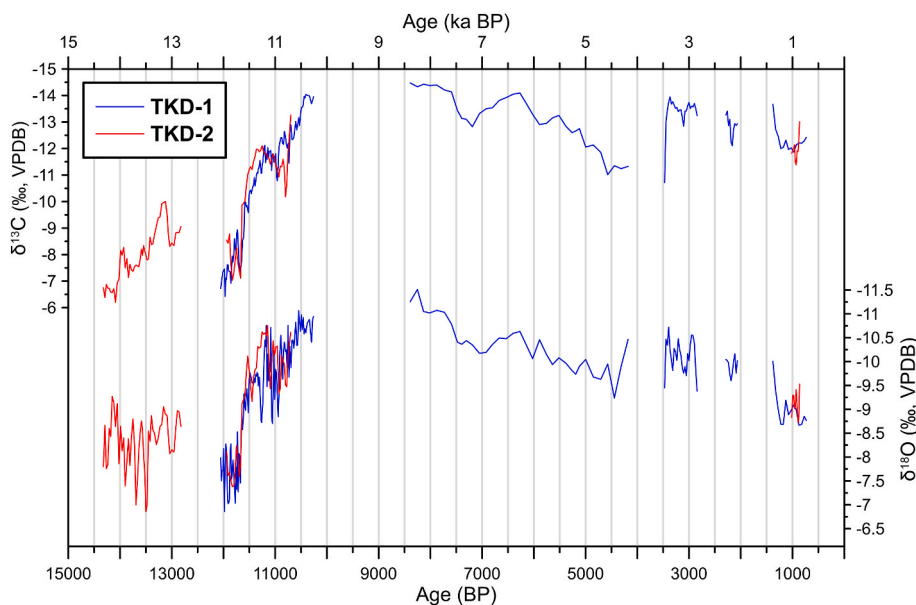
Fig. 5. Stable-isotope records from Tham Khao Dang Cave.

monthly $\delta^{18}O_p$ values between 2016 and 2017 from Uthai Thani province (approximately 50 km from the study site) show a negative correlation ($r = -0.84$, n = 24, $p < 0.0001$) between monthly mean $\delta^{18}O_p$ values and precipitation amount (Chawchai et al., 2020). A number of other factors can also influence speleothem $\delta^{18}O$ values, such as seasonality, temperature, and large-scale atmospheric circulation effects on $\delta^{18}O_p$ values (Liu et al., 2020). However, we agree with Li et al. (2022) and Buckingham et al. (2022) that consistency of speleothem $\delta^{18}O$ patterns across the broad ASM region is compelling evidence for common control factors: changes in the intensity and influence of different monsoon systems, with resultant impact on precipitation. Therefore, we interpret the speleothem $\delta^{18}O$ values as mainly reflecting seasonal or annual averages of local $\delta^{18}O_p$ values, influenced heavily by monsoon intensity, with lower $\delta^{18}O$ values indicating a higher amount of precipitation. Previously-conducted HYSPLIT analysis has revealed that, due to its location on the west side of the monsoon intersection zone and pathway of the ISM (Fig. 6), precipitation is brought to the cave primarily by the ISM (>85 %), with a minor (<15 %) contribution from the WNPSM (Chawchai et al., 2020). In-depth testing of the climatic significance of speleothem $\delta^{18}O$ values in the nearby Khao Prae Cave (Chawchai et al., 2020) and the accordance of the TKD records with other speleothem $\delta^{18}O$ records across the entire ASM region (see below) supports our interpretation.

The interpretation of speleothem $\delta^{13}C$ values is more complex with a vast range of factors. At Tham Khao Dang, speleothem $\delta^{13}C$ values range from -14.5 ‰ to -6.4 ‰ (average = -11.7 ‰) in TKD-1 and -13.6 to -6.2 ‰ (average = -9.6 ‰) in TKD-2, suggesting C_3 plants were always dominant above the cave (as today: Marod et al., 1999). Wetter and drier conditions at a cave site can be distinguished using $\delta^{13}C$ values indicating the prevalence of C_3 and C_4 plants; C_4 plants are adapted to warmer and drier climates, with ~14 ‰ higher $\delta^{13}C$ values than C_3 plants (Genty et al., 2001; Henderson et al., 1992). Even if C_3 plants

were always dominant, previous studies suggest that $\delta^{13}C$ values can be indicative of precipitation amount, with more precipitation enhancing biological activity (plants and microbes) and vegetation density above the cave (both resulting in higher soil pCO_2), as well as lowering the amount of prior calcite precipitation (PCP), which both lead to lower speleothem $\delta^{13}C$ values (Chawchai et al., 2020; Fohlmeister et al., 2020; McDermott et al., 2006). This is supported by visual similarities and strong Pearson correlations between $\delta^{18}O$ and $\delta^{13}C$ values in both TKD-1 ($r = 0.87$, n = 200, $p < 0.0001$) and TKD-2 ($r = 0.81$, n = 113, $p < 0.0001$), suggesting a common influence.

To understand the spatial extent of the climate changes revealed by the TKD speleothems and changes in neighboring regions, we compare a stacked composite $\delta^{18}O$ record from the two TKD speleothems to other paleoclimate records, most of which are representative of summer monsoon intensity and resultant precipitation from SEA (locations shown in Fig. 1).

5. Discussion

5.1. The Bølling–Allerød interstadial

The earliest data from Tham Khao Dang Cave comes from TKD-2, which had a period of formation between 14,321 and 12,824 BP. Chronologically, this corresponds to the Bølling–Allerød interstadial, a period of warmer conditions reflected by higher $\delta^{18}O$ values in the Greenland ice cores, dated to 14,642–12,896 BP (Buizert et al., 2014; Rasmussen et al., 2006, 2014). During this period, age uncertainties are relatively high in the TKD record, with an average of ±592 years (Fig. 4, Table 2), so we avoid an in-depth discussion of shorter-term events. There are two things of note in this phase. Firstly, $\delta^{18}O$ and $\delta^{13}C$ values are overall high but lower than in the YD, reflecting a monsoon weaker than the Holocene but stronger than the YD (Fig. 5). Secondly, this is the only period without a correlation between the TKD isotopes ($r = 0.20$, n = 51, $p > 0.05$). Whilst both isotopes have a trend towards lower values, this is only very slight in the $\delta^{18}O$ values and much more distinct in the $\delta^{13}C$ values, which reach their lowest (-10.0 ‰) at 13,123 BP (Fig. 5). These different responses may result from a delayed vegetation response to the onset of the Bølling-Allerød. We observe the same trend in EASM records extending from eastern China (e.g., Hulu: Wang et al., 2001) to western Indonesia (Tangga: Wurtzel et al., 2018) and Borneo (e.g., Gunung Mulu: Buckingham et al., 2022) (Fig. 7). This trend in many SEA speleothem $\delta^{18}O$ records is paralleled by lower $\delta^{18}O$ values in the NGRIP record, potentially resulting from a decrease in marine $\delta^{18}O$ values associated with glacial melting (Wang et al., 2001). The new TKD record is the first evidencing such a trend in the ISM region.

5.2. The termination of the younger Dryas

Both speleothems have a period of formation starting around 12,000 BP that begins with some of the highest isotope values and the strongest correlations between $\delta^{18}O$ and $\delta^{13}C$ values: TKD-1 ($r = 0.91$, n = 116, $p < 0.0001$) and TKD-2 ($r = 0.95$, n = 47, $p < 0.0001$). Based on the StalAge age model, this growth phase has low average age uncertainties in TKD-1 (±148 years) when compared to TKD-2 (±252 years) and exhibits a significant decrease in isotope values: ~3 ‰ for $\delta^{18}O$ and ~7 ‰ for $\delta^{13}C$ values. This decrease corresponds in time with the termination of the YD (Fig. 5). Through a visual assessment (VA hereafter), we observe a rapid shift in both sets of isotopes from both TKD speleothems centered on 11,700–11,650 BP (Supplementary Fig. S1). A significant decrease in isotope values during the YD termination is comparable with previously published monsoonal speleothem records (Figs. 7 and 8). The YD terminated with a sudden warming that likely originated in Antarctica prior to 11,900 BP, followed 200–300 years later in the North Atlantic (NGRIP: 11,700–11,610 BP) (Cheng et al., 2020; Rasmussen et al., 2014; WAIS Divide Project Members, 2015, 2013). The exact nature, timing, and duration, of the YD termination in different regions
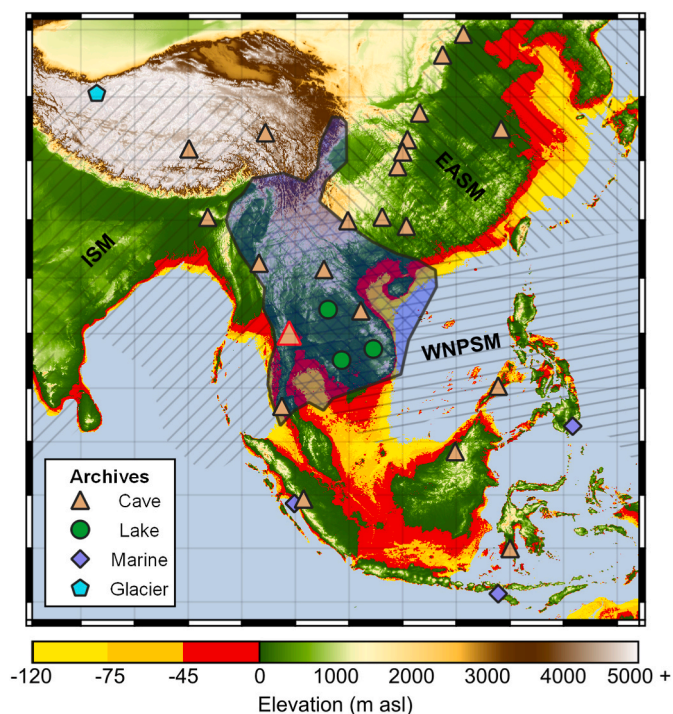

Fig. 6. Dashed lines reflect the influence of the different ASM subsystems, with the monsoon intersection zone highlighted in blue (Cheng et al., 2012b; Hamilton et al., 2019; Li et al., 2022; Wang and LinHo, 2002). Elevation data from the GEBCO Compilation Group (2023) is clipped below modern sea level to simulate the extent of the Sundaland continent during the YD (-45 m), BA Interstadial (-75 m), and Last Glacial Maximum (-120 m) (Leknettip et al., 2023). Archive labels are removed for clarity, see Fig. 1.
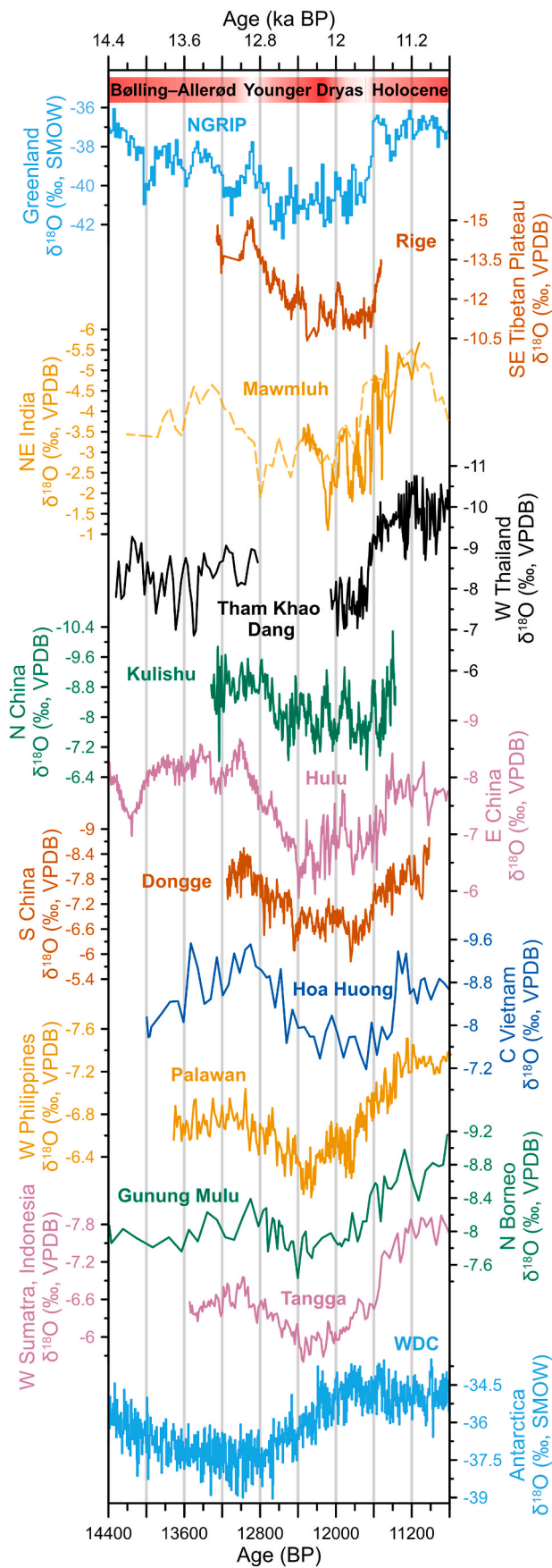
Fig. 7. The Pleistocene Tham Khao Dang Cave δ¹⁸O stack record compared to select paleoclimate records. More positive δ¹⁸O values in the NGRIP and WDC ice core records reflect higher temperatures in Greenland and Antarctica, respectively (Rasmussen et al., 2014; Seierstad et al., 2014; WAIS Divide Project Members, 2015, 2013). The remainder are speleothem δ¹⁸O records plotted inverse so that up in the figure corresponds to higher monsoon intensity and precipitation amount. These records are from Rige (Li et al., 2022), Mawmluh (1) (Dutt et al., 2015) and (3) (Cheng et al., 2020), Tham Khao Dang (this study), Kulishu (Cheng et al., 2020; Ma et al., 2012), Hulu (Wang et al., 2001), Dongge (Cheng et al., 2020; Dykoski et al., 2005), Hoa Huong (Patterson et al., 2023), Palawan (Partin et al., 2015), Gunung Mulu (Buckingham et al., 2022), and Tangga (Wurtzel et al., 2018) caves. Locations in Fig. 1 and 6.

of SEA are still under scrutiny (e.g., Buckingham et al., 2022; Cheng et al., 2020; Kuang et al., 2021; Partin et al., 2015; Patterson et al., 2023). In the following section, we preferentially utilize the results of BCP to quantitatively assess chronological differences in the start and end dates of the YD termination, as well as the most significant short-term shift. We are confident in the accuracy of the BCP method as the results are similar to our own VAs (Fig. 8 and Supplementary Table S2) and to established/well-evidenced YD terminations, such as in the NGRIP δ¹⁸O record (VA: 11,700–11,610 BP/BCP: 11,690–11,610 BP) and Palawan Cave δ¹⁸O record (VA: 11,790–11,360 BP/BCP: 11, 796–11,358 BP) (Partin et al., 2015; Rasmussen et al., 2014). However, of the total eighteen records, the BCP method only identified start, end, and shift dates in three; therefore, we revert to a VA for some records.

The termination of the YD appears to start early and occur relatively rapidly in the TKD records. Only BCP of the TKD-1 δ¹³C record provided start (11,702 ± 72 BP) and end (11,589 ± 74 BP) dates; the other records produced single BCPs at 11,660 BP (TKD-1 δ¹⁸O) and 11,641 BP (TKD-2 δ¹⁸O and δ¹³C) that correspond to the largest shift of the termination. VA of TKD-1 δ¹⁸O indicates a start date of 11,674 BP and an end date of 11,603 BP (see Supplementary Fig. S1). We will utilize this record for comparison as the other records we assess are also δ¹⁸O and TKD-1 has a higher resolution and stronger chronology.

The termination observed in TKD is very abrupt when compared to other tropical hydroclimate records, which average 274 years in a synthesis by Partin et al. (2015). Below, we discuss several distinct groupings for the timing and duration of the YD termination (visible in Fig. 8): (1) Indian Summer Monsoon region, (2) northern China, (3) central eastern China, (4) southern China, (5) eastern mainland SEA, and (6) Maritime SEA.

If precipitation at TKD is primarily driven by the ISM, we would expect to see other records influenced by that monsoon subsystem to show similar patterns, but this is currently unclear (Supplementary Fig. S2). There are several records from Mawmluh Cave (NE India) covering this period. Though, these are in disagreement as to the timing and duration of the YD termination. In the newest record, from Cheng et al. (2020), the highest probability change points suggest a termination from 11,514 to 11,336 BP, with a rapid change at 11,508 BP (Mawmluh (3) in Fig. 8). However, this record fluctuates intensely (Fig. 7) with 21 change points above the 0.7 probability threshold between 12,137 and 11,336 BP. This makes the YD termination hard to identify in this record, which starts changing at either 11,714 or 11,636 BP (see Fig. 7, this paper and Fig. 2 in Cheng et al. (2020)). Two other records from the same cave suggest an earlier YD termination, with a single BCP at 11,708 BP (Mawmluh (1) in Fig. 8) (Dutt et al., 2015) and a rapid change between 11,669 and 11,603 BP (Mawmluh (2) in Fig. 8) (Berkelhammer et al., 2012). A precisely-dated ISM record, from Rige Cave (SE Tibetan Plateau), possibly shows a short termination of the YD, dated by BCP to 11,698–11,585 BP (Li et al., 2022). However, it is important to note that the Rige record ends at 11,520 BP, so it is possible that the termination continued past this point.

There are a large number of speleothem δ¹⁸O records from China (Zhang et al., 2018), which show a varied timing and duration of the YD termination by region (Figs. 7 and 8, Supplementary Fig. S3). In
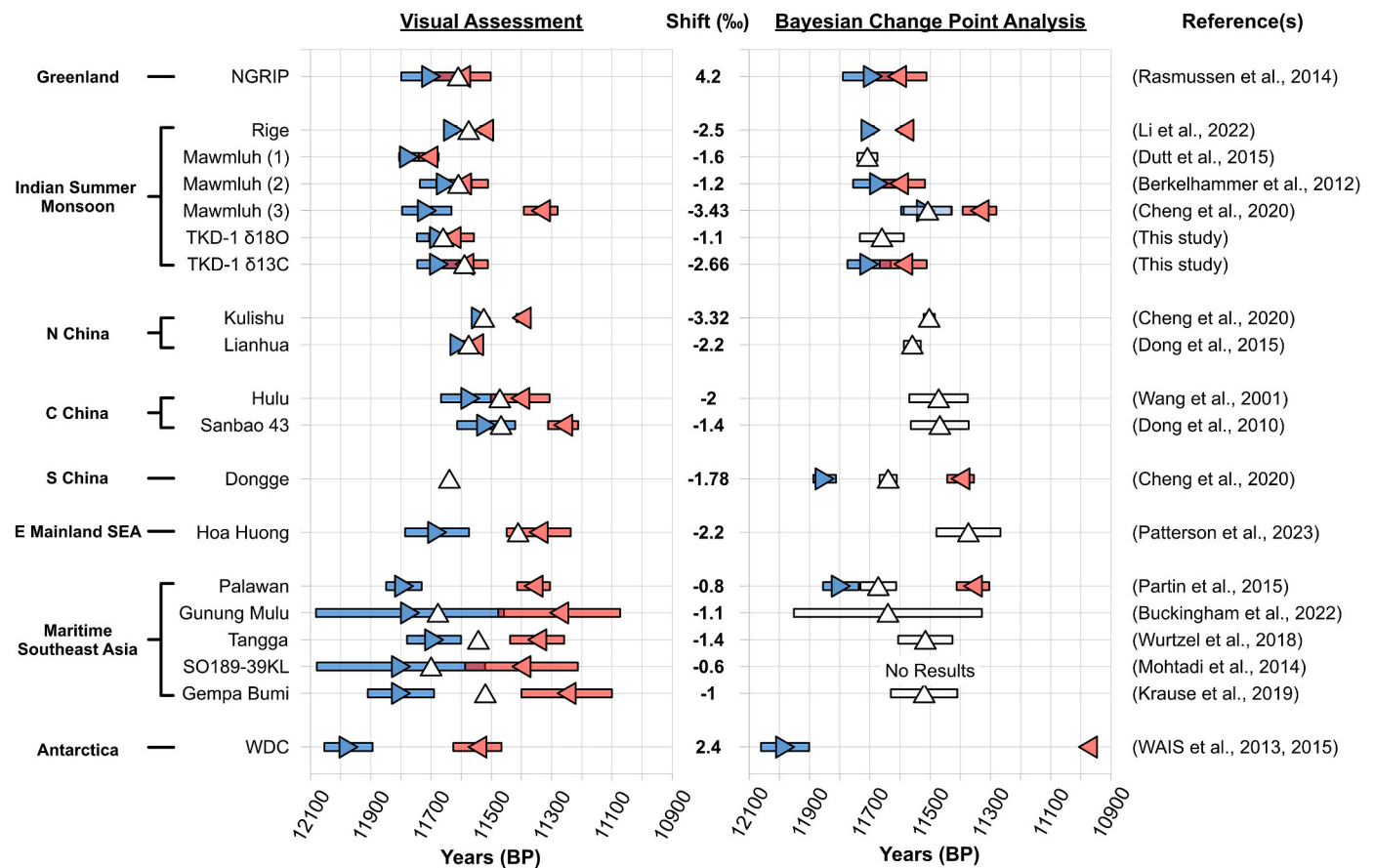
Fig. 8. Timing of the Younger Dryas Termination, based on a visual assessment (left) and Bayesian Change Point Analysis (right). Dates of the start (blue), end (red) and most rapid shift (white) are displayed, along with their age uncertainties (colored bars), taken from the age-models of the original publications where available, otherwise from the closest absolute age (details in Supplementary Table S2).

northern China, speleothem $\delta^{18}O$ records demonstrate YD terminations with a shift dated later, for example at Kulishu (11,503 BP) and Lianhua (11,559 BP) caves (Cheng et al., 2020; Dong et al., 2015; Ma et al., 2012). In central eastern China, the rapid shift comes later still, as evidenced by the Hulu (11,472 BP) and Sanbao-43 (11,468 BP), $\delta^{18}O$ records (Dong et al., 2010; Wang et al., 2001). A rapid shift just after 11,500 BP is mirrored by records from nearby caves: Jintawan and Hailuo (Chen et al., 2023; Cosford et al., 2010). Further south, speleothem hydroclimate proxies (Mg/Ca and $\delta^{13}C$) from Hoa Huong Cave, central Vietnam, do not show a YD termination. However, $\delta^{18}O$ values from the same speleothem have a rapid shift of ~1.5 ‰, centered on 11,373 BP, much later than other records (Patterson et al., 2023). Interestingly, the Dongge Cave record from southern China details a longer YD termination that starts earlier; BCP finds a transition in the $\delta^{18}O$ values at 11,639 BP but as part of a longer decreasing trend (11,850–11,399 BP) (Cheng et al., 2020; Dykoski et al., 2005). However, this early start is possibly just an artefact of the BCP analyses, from VA it is hard to identify the true start: it could arguably be anytime between 11,850 and 11,615 BP (Fig. 7 and Supplementary Fig. S3). RAMPFIT and BREAKFIT analyses by Cheng et al. (2020) date this to 11,710 and 11,770 BP, respectively. This YD termination is more similar to Maritime SEA than to other EASM records (Fig. 8). All five of the records across this broad region covering the YD termination (Palawan, Gunung Mulu, Tangga, SO189-39 KL, and Gempa Bumi) show earlier-starting and longer-lasting YD terminations (Buckingham et al., 2022; Krause et al., 2019; Mohtadi et al., 2014; Partin et al., 2015; Wurtzel et al., 2018). For example, in Palawan, Philippines (BCP: 11,796–11,358 BP) and Gempa Bumi Cave, Sulawesi, Indonesia (VA: 11,800–11,250 BP); for the remainder, see Figs. 7 and 8, Supplementary Fig. S4, and Supplementary Table S2. This occurs despite

Palawan being influenced by the WNPSM and there being entirely different controls in the regions further south.

The TKD record YD termination lasting around 70 years (11,674–11,603 BP), with a rapid increase at 11,660 BP, suggests the ISM responds faster and has an earlier rapid increase when compared to EASM records, which were previously deemed coeval (Cheng et al., 2012a). This pattern, which is supported by other ISM records, holds true even if the TKD shift was brought forward the maximum possible age uncertainty of 73 years. Records influenced by the EASM and/or WNPSM, exhibit different responses where more northern records tend to have earlier rapid shifts. EASM (Chinese) records exhibit their most extreme shift more than 100 years later in the north, at ~11,560 and 11,500 BP, and around 200 years later to the south (~11,470 BP). In the monsoon intersection zone, the shift is delayed further, occurring ~11,370 BP. The only record covering the YD termination in southern China (Dongge Cave) has its most rapid shift at 11,639 BP but as part of a much longer trend possibly starting prior to the NGRIP $\delta^{18}O$ shift at 11,690 BP. In Maritime SEA, all records also have more gradual YD terminations (as previously identified by Partin et al., 2015) that initiate earlier than in the North Atlantic. This supports the hypothesis of Cheng et al. (2020) that the YD termination had an Antarctica/Southern Hemisphere origin but opposes a western tropical Pacific origin as early as 12,300 BP. Several speleothem records from the ISM (e.g., Rige, Mawmluh) and EASM region (e.g., Hulu, Dongge) also have higher $\delta^{18}O$ values in the period 12,400–12,200 BP that decline over the YD (Fig. 7), this is unrelated to the termination. A Southern Hemisphere origin is also supported by the Antarctica WDC $\delta^{18}O$ record, which contains the earliest evidence for the start of the YD termination, dated to 11,981 BP with BCP (WAIS Divide Project Members, 2015, 2013). If these differences in

timing are true, they pose two important questions about the propagation of the YD termination: (1) why would western mainland SEA, influenced primarily by the ISM, respond faster when compared to EASM regions in north and central China? And (2) if Southern Hemisphere, maritime SEA and southern Chinese changes precede those in the North Atlantic, what mechanism(s) can explain this?

Overall, the underlying dynamics for the propagation of the termination between regions are still poorly understood; however, several key theories exist. The termination of the YD possibly resulted from increasing atmospheric CO_2 concentrations since the start of the YD (242 ppm at 12,870 BP), which reached a threshold of a 15-ppm increase by 11,900 BP (257 ppm) (Marcott et al., 2014; Zhang et al., 2017). Alternatively, or perhaps in tandem, a switch to a "La Niña-like" state from 11,900 BP or earlier (Cheng et al., 2020; Stott et al., 2002), could have strengthened the ASM in two ways. First, such a state can initiate a positive Indian Ocean Dipole (IOD) pattern via SST changes, which drives the ITCZ further north and enhances ISM intensity (Cai et al., 2021; Cherchi et al., 2021; Hrudya et al., 2021; Hu et al., 2023). Second, colder temperatures in the equatorial Pacific might have resulted in a warmer NH through interhemispheric heat redistribution (Bakker et al., 2017; Koutavas et al., 2002). This would occur via a gradual shift in the AMOC that reached a tipping point ~11,700 BP, causing a strong AMOC mode to return and rapidly heat the North Atlantic (Cheng et al., 2020; McManus et al., 2004; Muschitiello et al., 2019). A strong AMOC can strengthen the ASM by shifting the ITCZ northwards, with westerlies playing a significant role in the propagation of this event from the North Atlantic to ASM regions (Chen et al., 2023; Kuang et al., 2021; Sun et al., 2012; Yuan et al., 2023).

Explaining the potential earlier response of the ISM to the YD termination is challenging as the relationship between the ISM and EASM is complicated and ever-changing, controlled by e.g., the El Niño–Southern Oscillation, IOD, atmospheric teleconnection patterns, and Eurasian snow extent (Ha et al., 2018). Here, we present several ideas for potential mechanisms or reasons, but further research is required to confirm the timing differences and develop a greater understanding of their cause(s). Perhaps the simplest explanation comes from the propagation of the event which, regardless of whether it spread via the IOD or AMOC, would impact the ISM first. The ISM/Indian Ocean has a much stronger influence on the EASM than vice-versa (Zhu et al., 1986), notably through alterations to the IOD, which subsequently influences the EASM via snow distribution over Eurasia (Ha et al., 2018; Kripalani et al., 2010), and by altering the strength of the westerlies in response to orbital forcing (Clemens et al., 1991; Yang et al., 2023). An additional contribution might come from another key control on ASM strength, the Tibetan Plateau (Fallah et al., 2016; Webster et al., 1998). The world's largest plateau enhances the land-ocean temperature contrast due to its cool temperatures, explained by high altitudes (low air pressure) and glaciers, and contributes significantly to broad regional monsoon dynamics, including ASM strength and the seasonal reversal of the summer/winter Asian/Australian monsoons (Fallah et al., 2016; Wu et al., 2007, 2012). Furthermore, the Tibetan Plateau potentially had an even greater impact during the YD due to significantly larger glaciers and cooler temperatures, which could also have influenced the extent of northward movement of the ITCZ and strength of the westerlies (Saha et al., 2019; Tschudi et al., 2003; Yan et al., 2023). Around 12,000 BP, the SEA ITCZ was contracted and had migrated southward, but subsequently shifted rapidly to its most northerly position in the last 30,000 years and expanded, driven primarily by AMOC variability (Yuan et al., 2023). As the Tibetan Plateau is closer in proximity to the Indian Ocean when compared to the source of the EASM, perhaps the eastern sea would have to get comparatively warmer to drive the same monsoon increase, causing the delay in response. Additionally, this delay, and differences to the western tropical Pacific, may have been enhanced further by the Sundaland shoreline (Fig. 6). Whilst the rate of sea level change is debated (Horton et al., 2005; Leknettip et al., 2023; Sarr et al., 2019; Sathiamurthy and Voris, 2006; Surakiatchai et al., 2018), it is clear that additional Sundaland landmass would still have been exposed during the YD termination compared to the Holocene. It is possible that the Indian Ocean and South China Sea were not as closely connected due to the lower sea level and the closest route for water transport was via the Timor Sea (see Fig. 6). This would lower the influence of the ISM (EASM) in the east (west) due to an increased degree of rainout, lower speleothem $\delta^{18}O$ values further away from the coast (Lachniet, 2009), and perhaps exacerbate temporal differences in climatic changes. One connected consideration here is the debate around the influence of ISM on Chinese speleothem $\delta^{18}O$ records, which Pausata et al. (2011) previously suggested to be dominant during Heinrich events. However, if this was the case during the YD termination, such a delayed response seems unlikely. Li et al. (2019) have already contested this, finding $\delta^{18}O$ variations in EASM records to be far larger than in ISM records and concluding that EASM strength is thus also an important control on these records. However, the fact that a response to the YD termination is visible in the $\delta^{18}O$ record from Hoa Huong Cave but not in the hydroclimate proxies (Mg/Ca and $\delta^{13}C$ values) (Patterson et al., 2023) supports a source effect or seasonality contribution to speleothem $\delta^{18}O$ records. This record, and another speleothem $\delta^{18}O$ record from Dongge Cave, both appear to show the YD termination starting before 11,700 BP (Dykoski et al., 2005; Patterson et al., 2023), perhaps indicating an ISM influence in southern China and eastern mainland SEA.

We believe differences in the timing of terminations are worth exploring further, and at finer spatial resolutions, to resolve their legitimacy and provide further insight into the propagation of such events globally.

5.3. The Holocene

The TKD samples covering the YD termination continued their growth into the early-Holocene, stopping at 10,260 BP (TKD-1) and 10,700 BP (TKD-2). Interestingly, monsoon intensity (as evidenced by the $\delta^{18}O$ values) did not peak immediately at the start of the Holocene and continued to decrease until at least the end of these samples at 740 BP. The lowest isotope values are observed at the start of the mid-Holocene section of TKD-1, at 8250 BP ($\delta^{18}O$) and 8389 BP ($\delta^{13}C$) (Figs. 5 and 9). The peak of the summer monsoon was thus either at this time, or occurred during the hiatus (10,250–8400 BP). Whilst it is often claimed that the Holocene monsoon intensity maximum follows summer insolation, there is actually a significant delay as the June Northern Hemisphere Insolation Curve (NHI) at 30° N peaks at 11,000 BP but is above 500 W/m^2 between 15,000 and 8000 BP (Berger and Loutre, 1991). This delay to the insolation peak (Fig. 9) likely results from the persistence of large ice sheets on land, which lowers the land-sea temperature gradient that drives monsoon intensity. The Mawmluh Cave $\delta^{18}O$ records suggest high monsoon intensity starting from 10,300 BP (Dutt et al., 2015), 9600 BP (Lechleitner et al., 2017), and 8400 BP (Berkelhammer et al., 2012), whilst another from nearby (Umsynrang Cave) peaks at 9000 BP (Breitenbach, 2010). Further south, the Klang Cave record also peaks earlier at 10,240 BP (Chawchai et al., 2021). This precedes the Holocene EASM peak, which in China occurs generally between 8000 and 7000 BP (Yang et al., 2019; Zhang et al., 2018, 2019). For example, the $\delta^{18}O$ record from Dongge Cave peaks at 7530 BP (Fig. 9) (Wang et al., 2005). Recently-published speleothem records from Central Vietnam (Hoa Huong and Thien Duong caves) pertain to autumn/winter monsoon intensity and thus do not follow the same pattern (Patterson et al., 2023; Wolf et al., 2023). A much later peak is observed in most records from Maritime SEA, between 6000 and 4000 BP. For example, see the Bukit Assam, Tangga, and Gempa Bumi cave $\delta^{18}O$ records in Fig. 9, which are more closely related to autumn insolation (Partin et al., 2007) and controlled by a range of other climate systems (Chen et al., 2016; Wurtzel et al., 2018).

Speleothem TKD-1 grew during the early- to mid-Holocene, between approximately 8389–4177 BP. Unfortunately, age uncertainties during this growth phase are high (±1052–2050 years, average = ±1408
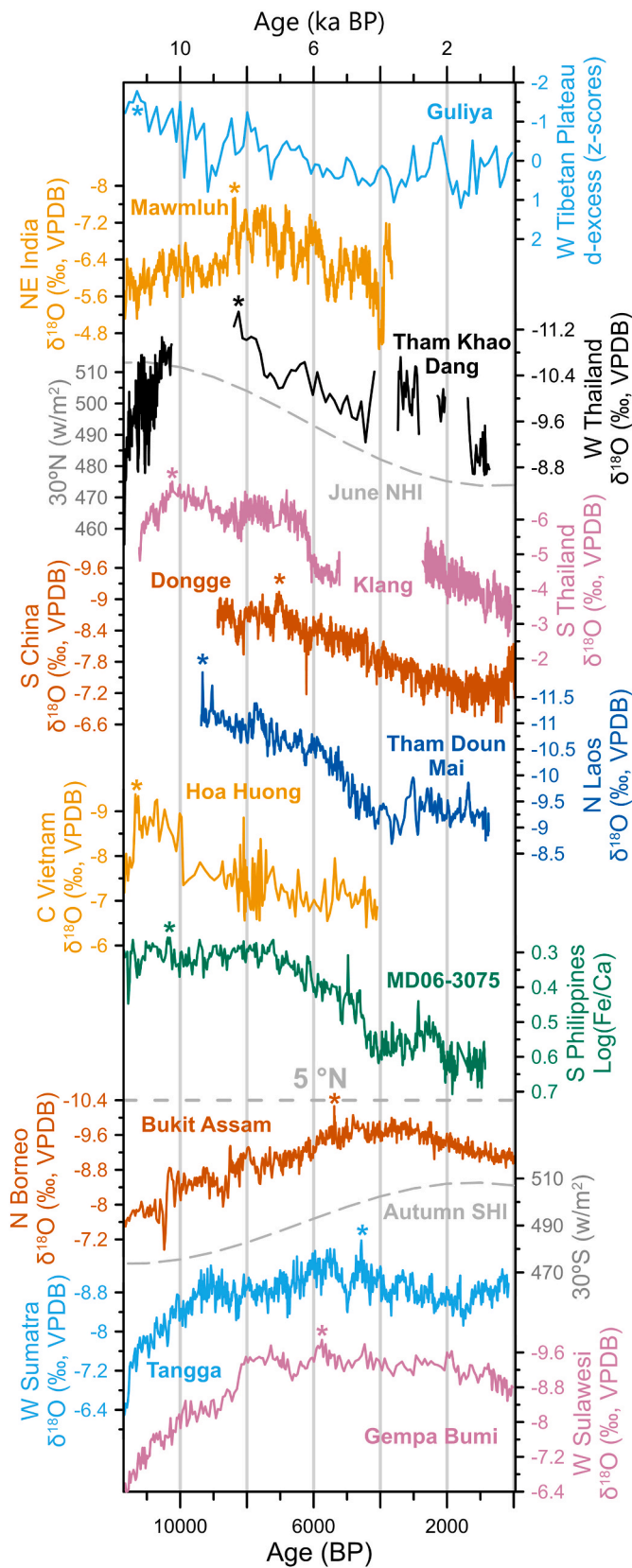
Fig. 9. Tham Khao Dang Cave δ^{18}O record during the Holocene compared to the June Northern Hemisphere Insolation (NHI) at 30°N and Autumn (Sep–Nov) Southern Hemisphere Insolation (SHI) at 30°S curves (Berger, 1978; Berger and Loutre, 1991) and other paleoclimate records plotted inverse so that up in the figure corresponds to higher monsoon intensity and precipitation amount. Ice core d-excess from Guliya (Thompson et al., 2022) and Fe/Ca ratios from marine core MD06-3075 (Fraser et al., 2014). All other records are δ^{18}O values from caves: Mawmluh (Berkelhammer et al., 2012), Dongge (Wang et al., 2005), Tham Doun Mai (Griffiths et al., 2020), Hoa Huong (Patterson et al., 2023), Tham Khao Dang (this study), Klang (Chawchai et al., 2021), Bukit Assam (Chen et al., 2016), Tangga (Wurtzel et al., 2018) and Gempa Bumi (Krause et al., 2019). Colored asterisks denote the lowest Holocene values for each record (monsoon peak/wettest conditions). Locations in Fig. 1 and 6.

years), which, in combination with a slow growth rate, makes the identification of shorter duration climatic changes challenging. However, one distinct pattern is clearly observable during this phase, even when the full age uncertainties are considered: a distinct Holocene increasing trend of both δ^{18}O and δ^{13}C values. This trend starts with the Middle Holocene growth phase (δ^{18}O = −11.51 ‰ at 8250 BP) and continues into the younger Late Holocene sections of TKD-1 (δ^{18}O = −8.77 ‰ at 734 BP), roughly following the June NHI curve at 30° N. There are three Late Holocene growth phases in TKD-1 and one very short growth phase in TKD-2 (Table 2 and Fig. 4). In these sections, age uncertainties average ± 216 years in TKD-1 and ±156 years in TKD-2. The increasing trend in these growth phases suggests a gradual reduction in monsoon intensity and drying of regional climate, continuing at least until the end of the TKD record at 734 BP (Figs. 5 and 9).

Two other caves from mainland SEA show this same strong trend, Klang Cave (Thai-Malay Peninsula) and Tham Doun Mai Cave (N Laos) (Chawchai et al., 2021; Griffiths et al., 2020; Tan et al., 2019), whilst in two others from Central Vietnam, Hoa Huong and Thien Duong caves, it is very weak (Patterson et al., 2023; Wolf et al., 2023). This can be explained by the predominance of autumn precipitation in the region, largely decoupled from monsoon intensity. In the summer monsoon-controlled regions of SEA, this trend is strong and ubiquitous, as has previously been identified in records across the ISM (Kaushal et al., 2018) and EASM (Yang et al., 2019; Zhang et al., 2019) regions. From ISM-impacted regions, d-excess from the Guliya ice core and speleothem δ^{18}O from Tianmen and Mawmluh caves show a reduction of monsoon intensity over the Holocene (Berkelhammer et al., 2012; Cai et al., 2012; Dutt et al., 2015; Lechleitner et al., 2017; Thompson et al., 2022). The same trend is evidenced in speleothem δ^{18}O records across the northern (e.g., Dongshiya, Sanbao and Lianhua caves) and southern (e.g., Dongge, Feilong and Fengyu caves) EASM regions (Dong et al., 2010, 2015; Duan et al., 2023; Dykoski et al., 2005; Li et al., 2017; Wang et al., 2005; Zhang et al., 2018).

In Maritime SEA, the pattern is not so uniform. An Fe/Ca record from marine core MD06-3075 off the southern coast of the Philippines represents precipitation-controlled sediment composition, influenced by the WNPSM, and exhibits a similar trend starting 7000 BP (Fraser et al., 2014). However, many Holocene paleoclimate records found south of 5° latitude instead show a decrease of δ^{18}O values that follows the YD termination and lasts until between 6000 and 4500 BP (Fig. 9). Speleothem δ^{18}O records from Bukit Assam (N Borneo), Tangga (W Sumatra) and Gempa Bumi (W Sulawesi) caves show decreases that start before the Holocene (Krause et al., 2019; Partin et al., 2007; Wurtzel et al., 2018). This same pattern is not reflected in marine core proxies of monsoon intensity, such as the SO189-39 KL record close to Tangga Cave or the GeoB10065-7 record off the south of Indonesia (Mohtadi et al., 2014; Steinke et al., 2014). As mentioned above, the speleothem records from this region are more closely related to autumn/winter insolation via the Australasian monsoon, which peaked later in the Holocene. A weak anti-correlation between the summer and winter monsoons of SEA has previously been explained by opposite impacts from seasonally migrating ITCZ (e.g., Griffiths et al., 2016; Sirocko et al.,

1996; Yancheva et al., 2007), although this relationship and cause has been disputed (e.g., Steinke et al., 2011).

In the Late Holocene, some smaller climatic shifts are detected, but these shorter-term changes are extremely tentative at this stage due to the high age uncertainties and low resolution of TKD samples in the Holocene. Higher-quality mid- to late-Holocene paleoclimate records from mainland SEA are required to verify or refute these shifts and establish their spatial extent.

6. Summary and conclusions

We present two speleothem records from Uthai Thani province, western Thailand, which are the first from western mainland SEA covering the Bølling–Allerød interstadial (TKD-2) and the first from western Thailand detailing the YD termination (TKD-1 and TKD-2) and mid-Holocene (TKD-1) periods. The stable isotope records are found to reflect monsoon intensity and precipitation amount, meaning key climate changes and trends can be revealed in the region.

Speleothem TKD-2 has a period of growth during the Bølling–Allerød interstadial, during which both δ^{18}O and δ^{13}C values have a trend towards lower values. This pattern is observed in summer monsoon records across Asia and likely results from a decrease in marine δ^{18}O values associated with glacial melting. The period with the strongest chronology and highest resolution is a period of growth covering the termination of the YD and the start of the Holocene. Both records indicate an abrupt termination of the YD, which is dated to 11,675–11,600 BP ($\pm$73 years) in the TKD-1 δ^{18}O record, superimposed on a long-term decreasing trend (wetter conditions). Bayesian Change Point Analysis of multiple paleoclimate records from SEA reveals divisions between ISM, EASM and Maritime SEA records. Maritime SEA records initiate their termination earlier at 11,800 BP, suggesting a Southern Hemisphere origin of the YD termination, and they are gradual, lasting several centuries. ISM records generally exhibit a rapid transition, starting around 11,700 BP, whilst northern EASM records still exhibit a rapid YD termination but delayed by ~100 years. Southern EASM records are delayed by ~200 years with a more drawn-out termination. Further research is still required to authenticate the earlier timing of the YD termination in ISM regions and to understand the mechanisms behind the broader regional timing differences. Some potentially important aspects include: the influence of ISM precipitation on Chinese speleothem δ^{18}O records, an ISM influence on EASM strength via the IOD, the role of the Tibetan Plateau in monsoon dynamics, and exposure of the Sundaland shoreline during lower sea levels.

The Holocene peak of the summer monsoon at TKD is at 8250 BP or earlier, this is a significant delay (of at least a millennia) from the June NHI peak at 11,000 BP, likely resulting from the persistence of large ice sheets on land lowering the land-sea temperature gradient. Comparison with other ASM records again reveals a faster response of the ISM to global changes when compared to the EASM. Following the ISM peak, dated sometime between 10,000 and 8000 BP, a distinct increasing trend in the stable isotope values is observable in TKD that endures until at least 750 BP. This trend occurs in all ISM and EASM records, closely following the summer NHI curve. Maritime SEA records show a different pattern, more closely paralleled by autumn and/or winter insolation due to the influence of different climate systems. Smaller climatic shifts in the Late Holocene are not identified due to high age uncertainties and low resolutions; we argue that resolving these events is an important next step for studies of climate-society interactions in the region.

Author contributions

Matthew J Jacobson: Formal Analysis, Software, Data Curation, Validation, Writing - Original Draft, Writing - Review & Editing, Visualization, **Sakonvan Chawchai**: Conceptualization, Investigation, Methodology, Resources, Writing - Review & Editing, Supervision, Funding Acquisition, Project Administration, **Denis Scholz**: Methodology, Validation, Resources, Writing - Review & Editing, Supervision, Funding Acquisition, Dana **F.C. Riechelmann**: Methodology, Validation, Resources, Writing - Review & Editing, Supervision, **Hubert Vonhof**: Methodology, Resources, Writing - Review & Editing, **Karin Holmgren**: Writing - Review & Editing, Supervision, **Xianfeng Wang**: Resources, Writing - Review & Editing, Funding Acquisition, **Guangxin Liu**: Investigation, Validation, Resources, Writing - Review & Editing.

Declaration of competing interest

The authors declare that they have no known competing financial interests or personal relationships that could have appeared to influence the work reported in this paper.

Data availability

Data has been uploaded as supplementary files and will also be available on the NOAA paleoclimate database.

Acknowledgements

Appendix A. Supplementary data

Supplementary data to this article can be found online at https://doi.org/10.1016/j.quascirev.2024.108597.

References

Bakker, P., Clark, P.U., Golledge, N.R., Schmittner, A., Weber, M.E., 2017. Centennial-scale holocene climate variations amplified by Antarctic ice sheet discharge. Nature 541, 72–76. https://doi.org/10.1038/nature20582.

Beck, H.E., Zimmermann, N.E., McVicar, T.R., Vergopolan, N., Berg, A., Wood, E.F., 2018. Present and future köppen-geiger climate classification maps at 1-km resolution. Sci. Data 5. https://doi.org/10.1038/sdata.2018.214.

Berger, A., 1978. Long-term variations of daily insolation and quaternary climatic changes. J. Atmos. Sci. 35, 2362–2367. https://doi.org/10.1175/1520-0469(1978)035<2362:LTVODI>2.0.CO, 2.

Berger, A., Loutre, M.F., 1991. Insolation values for the climate of the last 10 million years. Quat. Sci. Rev. 10, 297–317. https://doi.org/10.1016/0277-3791(91)90033-Q.

Berkelhammer, M., Sinha, A., Stott, L., Cheng, H., Pausata, F.s. r., Yoshimura, K., 2012. An abrupt shift in the Indian monsoon 4000 Years ago. In: Climates, Landscapes, and Civilizations. American Geophysical Union (AGU), pp. 75–88. https://doi.org/10.1029/2012GM001207.

Bird, M.I., Taylor, D., Hunt, C., 2005. Palaeoenvironments of insular Southeast Asia during the last glacial period: a savanna corridor in Sundaland? Quat. Sci. Rev. 24, 2228–2242. https://doi.org/10.1016/j.quascirev.2005.04.004.

Breitenbach, S., 2010. Changes in Monsoonal Precipitation and Atmospheric Circulation during the Holocene Reconstructed from Stalagmites from Northeastern India. University of Potsdam, Potsdam, Germany.

Buckingham, F.L., Carolin, S.A., Partin, J.W., Adkins, J.F., Cobb, K.M., Day, C.C., Ding, Q., He, C., Liu, Z., Otto-Bliesner, B., Roberts, W.H.G., Lejau, S., Malang, J., 2022. Termination 1 millennial-scale rainfall events over the Sunda Shelf. Geophys. Res. Lett. 49, e2021GL096937 https://doi.org/10.1029/2021GL096937.

Buizert, C., Gkinis, V., Severinghaus, J.P., He, F., Lecavalier, B.S., Kindler, P., Leuenberger, M., Carlson, A.E., Vinther, B., Masson-Delmotte, V., White, J.W.C., Liu, Z., Otto-Bliesner, B., Brook, E.J., 2014. Greenland temperature response to climate forcing during the last deglaciation. Science 345, 1177–1180. https://doi.org/10.1126/science.1254961.

Büntgen, U., 2022. Scrutinizing tree-ring parameters for Holocene climate reconstructions. WIREs Clim. Change 13, e778. https://doi.org/10.1002/wcc.778.

Cai, W., Wang, G., Li, Z., Zheng, X., Yang, K., Ng, B., 2021. Chapter 21 - response of the positive Indian Ocean dipole to climate change and impact on Indian summer monsoon rainfall. In: Chowdary, J., Parekh, A., Gnanaseelan, C. (Eds.), Indian Summer Monsoon Variability. Elsevier, pp. 413–432. https://doi.org/10.1016/B978-0-12-822402-1.00010-7.

Cai, Y., Zhang, H., Cheng, H., An, Z., Lawrence Edwards, R., Wang, X., Tan, L., Liang, F., Wang, J., Kelly, M., 2012. The Holocene Indian monsoon variability over the southern Tibetan Plateau and its teleconnections. Earth Planet Sci. Lett. 335 (336), 135–144. https://doi.org/10.1016/j.epsl.2012.04.035.

Chabangborn, A., Brandefelt, J., Wohlfarth, B., 2014. Asian monsoon climate during the Last Glacial Maximum: palaeo-data–model comparisons. Boreas 43, 220–242. https://doi.org/10.1111/bor.12032.

Chawchai, S., Chabangborn, A., Fritz, S., Väliranta, M., Mörth, C.-M., Blaauw, M., Reimer, P.J., Krusic, P.J., Löwemark, L., Wohlfarth, B., 2015. Hydroclimatic shifts in northeast Thailand during the last two millennia – the record of Lake Pa Kho. Quat. Sci. Rev. 111, 62–71. https://doi.org/10.1016/j.quascirev.2015.01.007.

Chawchai, S., Chabangborn, A., Kylander, M., Löwemark, L., Mörth, C.-M., Blaauw, M., Klubseang, W., Reimer, P.J., Fritz, S.C., Wohlfarth, B., 2013. Lake Kumphawapi – an archive of Holocene palaeoenvironmental and palaeoclimatic changes in northeast Thailand. Quat. Sci. Rev. 68, 59–75. https://doi.org/10.1016/j.quascirev.2013.01.030.

Chawchai, S., Liu, G., Bissen, R., Jankham, K., Paisonjumlongsri, W., Kanjanapayont, P., Chutakositkanon, V., Choowong, M., Pailoplee, S., Wang, X., 2018. Stalagmites from western Thailand: preliminary investigations and challenges for palaeoenvironmental research. Boreas 47, 367–376. https://doi.org/10.1111/bor.12299.

Chawchai, S., Liu, G., Bissen, R., Scholz, D., Riechelmann, D.F.C., Vonhof, H., Mertz-Kraus, R., Chiang, H.-W., Tan, L., Wang, X., 2020. Hydroclimate variability of western Thailand during the last 1400 years. Quat. Sci. Rev. 241, 106423 https://doi.org/10.1016/j.quascirev.2020.106423.

Chawchai, S., Tan, L., Löwemark, L., Wang, H.-C., Yu, T.-L., Chung, Y.-C., Mii, H.-S., Liu, G., Blaauw, M., Gong, S.-Y., Wohlfarth, B., Shen, C.-S., 2021. Hydroclimate variability of central Indo-Pacific region during the Holocene. Quat. Sci. Rev. 253, 106779 https://doi.org/10.1016/j.quascirev.2020.106779.

Chen, S., Hoffmann, S.S., Lund, D.C., Cobb, K.M., Emile-Geay, J., Adkins, J.F., 2016. A high-resolution speleothem record of western equatorial Pacific rainfall: implications for Holocene ENSO evolution. Earth Planet Sci. Lett. 442, 61–71. https://doi.org/10.1016/j.epsl.2016.02.050.

Chen, X., Zhang, H., Griffiths, M.L., Peng, X., Yang, L., Yu, M., Huang, J., Xue, S., Cheng, H., Chen, S., 2023. Northern high-latitude sea ice variation linked with East Asian monsoon anomalies during the Younger Dryas. Palaeogeogr. Palaeoclimatol. Palaeoecol. 626, 111702 https://doi.org/10.1016/j.palaeo.2023.111702.

Cheng, H., Lawrence Edwards, R., Shen, C.C., Polyak, V.J., Asmerom, Y., Woodhead, J., Hellstrom, J., Wang, Y., Kong, X., Spötl, C., Wang, X., Calvin Alexander, E., 2013. Improvements in 230 Th dating, 230 Th and 234 U half-life values, and U-Th isotopic measurements by multi-collector inductively coupled plasma mass spectrometry. Earth Planet Sci. Lett. 371 (372), 82–91. https://doi.org/10.1016/j.epsl.2013.04.006.

Cheng, H., Sinha, A., Wang, X., Cruz, F.W., Edwards, R.L., 2012a. The global paleomonsoon as seen through speleothem records from Asia and the Americas. Clim. Dynam. 39, 1045–1062. https://doi.org/10.1007/s00382-012-1363-7.

Cheng, H., Zhang, H., Spötl, C., Baker, J., Sinha, A., Li, H., Bartolomé, M., Moreno, A., Kathayat, G., Zhao, J., Dong, X., Li, Y., Ning, Y., Jia, X., Zong, B., Ait Brahim, Y., Pérez-Mejías, C., Cai, Y., Novello, V.F., Cruz, F.W., Severinghaus, J.P., An, Z., Edwards, R.L., 2020. Timing and structure of the Younger Dryas event and its underlying climate dynamics. Proc. Natl. Acad. Sci. USA 117, 23408–23417. https://doi.org/10.1073/pnas.2007869117.

Cheng, H., Zhang, P.Z., Spötl, C., Edwards, R.L., Cai, Y.J., Zhang, D.Z., Sang, W.C., Tan, M., An, Z.S., 2012b. The climatic cyclicity in semiarid-arid central Asia over the past 500,000 years. Geophys. Res. Lett. 39 https://doi.org/10.1029/2011GL050202.

Cherchi, A., Terray, P., Ratna, S.B., Sankar, S., Sooraj, K.P., Behera, S., 2021. Chapter 8 - Indian Ocean Dipole influence on Indian summer monsoon and ENSO: a review. In: Chowdary, J., Parekh, A., Gnanaseelan, C. (Eds.), Indian Summer Monsoon Variability. Elsevier, pp. 157–182. https://doi.org/10.1016/B978-0-12-822402-1.00011-9.

Clark, P.U., Shakun, J.D., Baker, P.A., Bartlein, P.J., Brewer, S., Brook, E., Carlson, A.E., Cheng, H., Kaufman, D.S., Liu, Z., Marchitto, T.M., Mix, A.C., Morrill, C., Otto-Bliesner, B.L., Pahnke, K., Russell, J.M., Whitlock, C., Adkins, J.F., Blois, J.L., Clark, J., Colman, S.M., Curry, W.B., Flower, B.P., He, F., Johnson, T.C., Lynch-Stieglitz, J., Markgraf, V., McManus, J., Mitrovica, J.X., Moreno, P.I., Williams, J.W., 2012. Global climate evolution during the last deglaciation. Proc. Natl. Acad. Sci. U. S. A 109, E1134–E1142. https://doi.org/10.1073/pnas.1116619109.

Clemens, S., Prell, W., Murray, D., Shimmield, G., Weedon, G., 1991. Forcing mechanisms of the Indian Ocean monsoon. Nature 353, 720–725. https://doi.org/10.1038/353720a0.

Cosford, J., Qing, H., Lin, Y., Eglington, B., Mattey, D., Chen, Y.G., Zhang, M., Cheng, H., 2010. The East asian monsoon during MIS 2 expressed in a speleothem δ18O record from Jintanwan cave, Hunan, China. Quat. Res. 73, 541–549. https://doi.org/10.1016/j.yqres.2010.01.003.

De Deckker, P., Tapper, N.J., van der Kaars, S., 2003. The status of the indo-pacific warm pool and adjacent land at the last glacial maximum. Global Planet. Change 35, 25–35. https://doi.org/10.1016/S0921-8181(02)00089-9.

Dettman, D.L., Lohmann, K.C., 1995. Microsampling carbonates for stable isotope and minor element analysis; physical separation of samples on a 20 micrometer scale. J. Sediment. Res. 65, 566–569. https://doi.org/10.1306/D426813F-2B26-11D7-8648000102C1865D.

Dong, J., Shen, C.-C., Kong, X., Wang, H.-C., Jiang, X., 2015. Reconciliation of hydroclimate sequences from the Chinese loess plateau and low-latitude East Asian summer monsoon regions over the past 14,500years. Palaeogeogr. Palaeoclimatol. Palaeoecol. 435, 127–135. https://doi.org/10.1016/j.palaeo.2015.06.013.

Dong, J., Wang, Y., Cheng, H., Hardt, B., Edwards, R.L., Kong, X., Wu, J., Chen, S., Liu, D., Jiang, X., Zhao, K., 2010. A high-resolution stalagmite record of the Holocene East Asian monsoon from Mt Shennongjia, central China. Holocene 20, 257–264. https://doi.org/10.1177/0959683609350393.

Duan, R., Li, T.-Y., Li, J.-Y., Spötl, C., Li, H.-C., Wang, H.-B., Cheng, H., Ning, Y.-F., Shen, C.-C., Zhou, J.-L., Chen, C.-J., Yu, T.-L., Edwards, R.L., Liu, Z.-Q., 2023. Karst-ecological changes during the middle and late Holocene in Southwest China revealed by δ18O and δ13C records in a stalagmite. Palaeogeogr. Palaeoclimatol. Palaeoecol. 111437 https://doi.org/10.1016/j.palaeo.2023.111437.

Dutt, S., Gupta, A.K., Clemens, S.C., Cheng, H., Singh, R.K., Kathayat, G., Edwards, R.L., 2015. Abrupt changes in Indian summer monsoon strength during 33,800 to 5500 years B. P. Geophys. Res. Lett. 42, 5526–5532. https://doi.org/10.1002/2015GL064015.

Dykoski, C.A., Edwards, R.L., Cheng, H., Yuan, D., Cai, Y., Zhang, M., Lin, Y., Qing, J., An, Z., Revenaugh, J., 2005. A high-resolution, absolute-dated Holocene and deglacial Asian monsoon record from Dongge Cave, China. Earth Planet Sci. Lett. 233, 71–86. https://doi.org/10.1016/j.epsl.2005.01.036.

Erdman, C., Emerson, J.W., 2008. Bcp: an R package for performing a bayesian analysis of change point problems. J. Stat. Software 23, 1–13. https://doi.org/10.18637/jss.v023.i03.

Fallah, B., Cubasch, U., Prömmel, K., Sodoudi, S., 2016. A numerical model study on the behaviour of Asian summer monsoon and AMOC due to orographic forcing of Tibetan Plateau. Clim. Dynam. 47, 1485–1495. https://doi.org/10.1007/s00382-015-2914-5.

Fohlmeister, J., Voarintsoa, N.R.G., Lechleitner, F.A., Boyd, M., Brandtstätter, S., Jacobson, M.J., Oster, J.L., 2020. Main controls on the stable carbon isotope composition of speleothems. Geochem. Cosmochim. Acta 279, 67–87. https://doi.org/10.1016/j.gca.2020.03.042.

Fraser, N., Kuhnt, W., Holbourn, A., Bolliet, T., Andersen, N., Blanz, T., Beaufort, L., 2014. Precipitation variability within the west pacific warm pool over the past 120 ka: evidence from the Davao Gulf, southern Philippines. Paleoceanography 29, 1094–1110. https://doi.org/10.1002/2013PA002599.

GEBCO Compilation Group, 2023. General Bathymetric Chart of the Oceans 2023 Grid. https://doi.org/10.5285/f98b053b-0cbc-6c23-e053-6c86abc0af7b.

Genty, D., Baker, A., Massault, M., Proctor, C., Gilmour, M., Pons-Branchu, E., Hamelin, B., 2001. Dead carbon in stalagmites: carbonate bedrock paleodissolution vs. ageing of soil organic matter. Implications for 13C variations in speleotherms. Geochem. Cosmochim. Acta 65, 3443–3457. https://doi.org/10.1016/S0016-7037(01)00697-4.

Gibert, L., Scott, G.R., Scholz, D., Budsky, A., Ferràndez, C., Ribot, F., Martin, R.A., Lería, M., 2016. Chronology for the Cueva Victoria fossil site (SE Spain): evidence for early Pleistocene Afro-iberian dispersals. J. Hum. Evol. 90, 183–197. https://doi.org/10.1016/j.jhevol.2015.08.002.

Griffiths, M.L., Johnson, K.R., Pausata, F.S.R., White, J.C., Henderson, G.M., Wood, C.T., Yang, H., Ersek, V., Conrad, C., Sekhon, N., 2020. End of green Sahara amplified mid- to late holocene megadroughts in mainland Southeast Asia. Nat. Commun. 11, 4204. https://doi.org/10.1038/s41467-020-17927-6.

Griffiths, M.L., Kimbrough, A.K., Gagan, M.K., Drysdale, R.N., Cole, J.E., Johnson, K.R., Zhao, J.-X., Cook, B.I., Hellstrom, J.C., Hantoro, W.S., 2016. Western Pacific hydroclimate linked to global climate variability over the past two millennia. Nat. Commun. 7, 11719 https://doi.org/10.1038/ncomms11719.

Ha, K.-J., Seo, Y.-W., Lee, J.-Y., Kripalani, R.H., Yun, K.-S., 2018. Linkages between the South and East Asian summer monsoons: a review and revisit. Clim. Dynam. 51, 4207–4227. https://doi.org/10.1007/s00382-017-3773-z.

Hamilton, R., Penny, D., Hua, Q., 2019. A 4700-year record of hydroclimate variability over the Asian monsoon intersection zone inferred from multi-proxy analysis of lake sediments. Global Planet. Change 174, 92–104. https://doi.org/10.1016/j.gloplacha.2018.12.009.

Henderson, S.A., von Caemmerer, S., Farquhar, G.D., 1992. Short-term measurements of carbon isotope discrimination in several C4 species. Aust. J. Plant Physiol. 19, 263–285.

Horton, B.P., Gibbard, P.L., Mine, G.M., Morley, R.J., Purintavaragul, C., Stargardt, J.M., 2005. Holocene sea levels and palaeoenvironments, Malay-Thai Peninsula, southeast Asia. Holocene 15, 1199–1213. https://doi.org/10.1191/0959683605hl891rp.

Hrudya, P.H., Varikoden, H., Vishnu, R., 2021. A review on the Indian summer monsoon rainfall, variability and its association with ENSO and IOD. Meteorol. Atmos. Phys. 133, 1–14. https://doi.org/10.1007/s00703-020-00734-5.

Hu, J., Dee, S., Parajuli, G., Thirumalai, K., 2023. Tropical pacific modulation of the asian summer monsoon over the last millennium in paleoclimate data assimilation reconstructions. J. Geophys. Res. Atmospheres 128, e2023JD039207. https://doi.org/10.1029/2023JD039207.

Kaushal, N., Breitenbach, S.F.M., Lechleitner, F.A., Sinha, A., Tewari, V.C., Ahmad, S.M., Berkelhammer, M., Band, S., Yadava, M., Ramesh, R., Henderson, G.M., 2018. The Indian summer monsoon from a speleothem δ18O perspective—a review. Quaternary 1, 29. https://doi.org/10.3390/quat1030029.

Koutavas, A., Lynch-Stieglitz, J., Marchitto, T.M., Sachs, J.P., 2002. El niño-like pattern in ice age tropical pacific sea surface temperature. Science 297, 226–230. https://doi.org/10.1126/science.1072376.

Krause, C.E., Gagan, M.K., Dunbar, G.B., Hantoro, W.S., Hellstrom, J.C., Cheng, H., Edwards, R.L., Suwargadi, B.W., Abram, N.J., Rifai, H., 2019. Spatio-temporal evolution of Australasian monsoon hydroclimate over the last 40,000 years. Earth Planet Sci. Lett. 513, 103–112. https://doi.org/10.1016/j.epsl.2019.01.045.

Kripalani, R.H., Oh, J.H., Chaudhari, H.S., 2010. Delayed influence of the Indian Ocean Dipole mode on the East Asia–West Pacific monsoon: possible mechanism. Int. J. Climatol. 30, 197–209. https://doi.org/10.1002/joc.1890.

Kuang, X., Schenk, F., Smittenberg, R., Hällberg, P., Zhang, Q., 2021. Seasonal evolution differences of east Asian summer monsoon precipitation between Bølling-Allerød and younger Dryas periods. Clim. Change 165, 19. https://doi.org/10.1007/s10584-021-03025-z.

Lachniet, M.S., 2009. Climatic and environmental controls on speleothem oxygen-isotope values. Quat. Sci. Rev. 28, 412–432. https://doi.org/10.1016/j.quascirev.2008.10.021.

Lan, J., Cheng, J., Chawchai, S., Liu, X., Cheng, P., Liu, Y., Leknettip, S., Yan, H., Sun, Y., Dong, J., Xu, H., Ma, X., Zhang, H., Lu, F., Ma, L., Tan, L., Liu, Z., 2023. Fundamental shift from summer to winter holocene rainfall regime in the tropics. Geophys. Res. Lett. 50, e2023GL102909 https://doi.org/10.1029/2023GL102909.

Lechleitner, F.A., Breitenbach, S.F.M., Cheng, H., Plessen, B., Rehfeld, K., Goswami, B., Marwan, N., Eroglu, D., Adkins, J., Haug, G., 2017. Climatic and in-cave influences on δ18O and δ13C in a stalagmite from northeastern India through the last deglaciation. Quat. Res. 88, 458–471. https://doi.org/10.1017/qua.2017.72.

Leknettip, S., Chawchai, S., Choowong, M., Mueller, D., Fülling, A., Preusser, F., 2023. Sand ridges from the coastal zone of southern Thailand reflect late quaternary sea-level history and environmental conditions in Sundaland. Quat. Sci. Rev. 316, 108264 https://doi.org/10.1016/j.quascirev.2023.108264.

Li, D., Tan, L., Cai, Y., Jiang, X., Ma, L., Cheng, H., Edwards, R.L., Zhang, H., Gao, Y., An, Z., 2019. Is Chinese stalagmite δ18O solely controlled by the Indian summer monsoon? Clim. Dynam. 53, 2969–2983. https://doi.org/10.1007/s00382-019-04671-x.

Li, H.-C., Bar-Matthews, M., Chang, Y.-P., Ayalon, A., Yuan, D.-X., Zhang, M.-L., Lone, M. A., 2017. High-resolution δ18O and δ13C records during the past 65 ka from Fengyu Cave in Guilin: variation of monsoonal climates in south China. Quat. Int., Environmental and Climatic Changes Inferred from Sedimentary Records on Asian Shelf Margins: Part II 441, 117–128. https://doi.org/10.1016/j.quaint.2016.08.048.

Li, Y., Pérez-Mejías, C., Zhao, J., Li, H., Zhang, H., Lu, J., Wang, J., Duan, P., Dong, X., Wang, H., Ning, Y., Qian, Z., Edwards, R.L., Cheng, H., 2022. Indian summer monsoon variations during the Younger Dryas as revealed by a laminated stalagmite record from the Tibetan Plateau. Quat. Sci. Rev. 278, 107375 https://doi.org/10.1016/j.quascirev.2022.107375.

Liu, G., Li, X., Chiang, H.-W., Cheng, H., Yuan, S., Chawchai, S., He, S., Lu, Y., Aung, L.T., Maung, P.M., Tun, W.N., Oo, K.M., Wang, X., 2020. On the glacial-interglacial variability of the Asian monsoon in speleothem δ18O records. Sci. Adv. 6, eaay8189 https://doi.org/10.1126/sciadv.aay8189.

Ma, Z.-B., Cheng, H., Tan, M., Edwards, R.L., Li, H.-C., You, C.-F., Duan, W.-H., Wang, X., Kelly, M.J., 2012. Timing and structure of the Younger Dryas event in northern China. Quat. Sci. Rev. 41, 83–93. https://doi.org/10.1016/j.quascirev.2012.03.006.

Marcott, S.A., Bauska, T.K., Buizert, C., Steig, E.J., Rosen, J.L., Cuffey, K.M., Fudge, T.J., Severinghaus, J.P., Ahn, J., Kalk, M.L., McConnell, J.R., Sowers, T., Taylor, K.C., White, J.W.C., Brook, E.J., 2014. Centennial-scale changes in the global carbon cycle during the last deglaciation. Nature 514, 616–619. https://doi.org/10.1038/nature13799.

Marod, D., Kutintara, U., Yarwudhi, C., Tanaka, H., Nakashisuka, T., 1999. Structural dynamics of a natural mixed deciduous forest in western Thailand. J. Veg. Sci. 10, 777–786. https://doi.org/10.2307/3237302.

McDermott, F., Schwarcz, H.P., Rowe, P.J., 2006. Isotopes in speleothems. In: Leng, M.J. (Ed.), Isotopes in Palaeoenvironmental Research, vol. 10. Springer, Dordrecht, The Netherlands, pp. 185–226.

McManus, J.F., Francois, R., Gherardi, J.-M., Keigwin, L.D., Brown-Leger, S., 2004. Collapse and rapid resumption of Atlantic meridional circulation linked to deglacial climate changes. Nature 428, 834–837. https://doi.org/10.1038/nature02494.

Mohtadi, M., Prange, M., Oppo, D.W., De Pol-Holz, R., Merkel, U., Zhang, X., Steinke, S., Lückge, A., 2014. North Atlantic forcing of tropical Indian Ocean climate. Nature 509, 76–80. https://doi.org/10.1038/nature13196.

Mudelsee, M., 2009. Break function regression. Eur. Phys. J. Spec. Top. 174, 49–63. https://doi.org/10.1140/epjst/e2009-01089-3.

Mudelsee, M., 2000. Ramp function regression: a tool for quantifying climate transitions. Comput. Geosci. 26, 293–307. https://doi.org/10.1016/S0098-3004(99)00141-7.

Muschitiello, F., D'Andrea, W.J., Schmittner, A., Heaton, T.J., Balascio, N.L., deRoberts, N., Caffee, M.W., Woodruff, T.E., Welten, K.C., Skinner, L.C., Simon, M. H., Dokken, T.M., 2019. Deep-water circulation changes lead North Atlantic climate during deglaciation. Nat. Commun. 10, 1272. https://doi.org/10.1038/s41467-019-09237-3.

Nguyen, H.T.T., Galelli, S., Xu, C., Buckley, B.M., 2022. Droughts, Pluvials, and Wet season timing across the Chao Phraya river basin: a 254-year monthly reconstruction from tree ring widths and δ18O. Geophys. Res. Lett. 49, e2022GL100442 https://doi.org/10.1029/2022GL100442.

Obert, J.C., Scholz, D., Felis, T., Brocas, W.M., Jochum, K.P., Andreae, M.O., 2016. 230Th/U dating of Last Interglacial brain corals from Bonaire (southern Caribbean)

using bulk and theca wall material. Geochem. Cosmochim. Acta 178, 20–40. https://doi.org/10.1016/j.gca.2016.01.011.

Partin, J.W., Cobb, K.M., Adkins, J.F., Clark, B., Fernandez, D.P., 2007. Millennial-scale trends in west Pacific warm pool hydrology since the Last Glacial Maximum. Nature 449, 452–455. https://doi.org/10.1038/nature06164.

Partin, J.W., Quinn, T.M., Shen, C.-C., Okumura, Y., Cardenas, M.B., Siringan, F.P., Banner, J.L., Lin, K., Hu, H.-M., Taylor, F.W., 2015. Gradual onset and recovery of the Younger Dryas abrupt climate event in the tropics. Nat. Commun. 6, 8061. https://doi.org/10.1038/ncomms9061.

Patterson, E.W., Johnson, K.R., Griffiths, M.L., Kinsley, C.W., McGee, D., Du, X., Pico, T., Wolf, A., Ersek, V., Mortlock, R.A., Yamoah, K.A., Bùi, T.N., Trần, M.X., Đỗ-Trọng, Q., Võ, T.V., Đinh, T.H., 2023. Glacial changes in sea level modulated millennial-scale variability of Southeast Asian autumn monsoon rainfall. Proc. Natl. Acad. Sci. USA 120, e2219489120. https://doi.org/10.1073/pnas.2219489120.

Pausata, F.S.R., Battisti, D.S., Nisancioglu, K.H., Bitz, C.M., 2011. Chinese stalagmite δ18O controlled by changes in the Indian monsoon during a simulated Heinrich event. Nat. Geosci. 4, 474–480. https://doi.org/10.1038/ngeo1169.

Penny, D., 2006. The holocene history and development of the Tonle Sap, Cambodia. Quat. Sci. Rev. 25, 310–322. https://doi.org/10.1016/j.quascirev.2005.03.012.

Pereira, J.J., Shaw, R., 2022. Southeast Asia: an outlook on climate change. In: Pereira, J. J., Zain, M.K., Shaw, R. (Eds.), Climate Change Adaptation in Southeast Asia, Disaster Risk Reduction. Springer Singapore, Singapore, pp. 1–24. https://doi.org/10.1007/978-981-16-6088-7_1.

Preechamart, S., Pumijumnong, N., Bräuning, A., Muangsong, C., Cai, B., Buajan, S., 2023. Inter-annual and intra-annual tree-ring oxygen isotope signals in response to monsoon rainfall in northwestern Thailand. Holocene 33, 335–346. https://doi.org/10.1177/09596836221138352.

R Core Team, 2023. R: A Language and Environment for Statistical Computing.

Rasmussen, S.O., Andersen, K.K., Svensson, A.M., Steffensen, J.P., Vinther, B.M., Clausen, H.B., Siggaard-Andersen, M.-L., Johnsen, S.J., Larsen, L.B., Dahl-Jensen, D., Bigler, M., Röthlisberger, R., Fischer, H., Goto-Azuma, K., Hansson, M.E., Ruth, U., 2006. A new Greenland ice core chronology for the last glacial termination. J. Geophys. Res. Atmospheres 111. https://doi.org/10.1029/2005JD006079.

Rasmussen, S.O., Bigler, M., Blockley, S.P., Blunier, T., Buchardt, S.L., Clausen, H.B., Cvijanovic, I., Dahl-Jensen, D., Johnsen, S.J., Fischer, H., Gkinis, V., Guillevic, M., Hoek, W.Z., Lowe, J.J., Pedro, J.B., Popp, T., Seierstad, I.K., Steffensen, J.P., Svensson, A.M., Vallelonga, P., Vinther, B.M., Walker, M.J.C., Wheatley, J.J., Winstrup, M., 2014. A stratigraphic framework for abrupt climatic changes during the Last Glacial period based on three synchronized Greenland ice-core records: refining and extending the INTIMATE event stratigraphy. Quat. Sci. Rev., Dating, Synthesis, and Interpretation of Palaeoclimatic Records and Model-data Integration: advances of the INTIMATE project(INTegration of Ice core. Marine and TErrestrial records, COST Action ES0907) 106, 14–28. https://doi.org/10.1016/j.quascirev.2014.09.007.

Richards, D.A., Dorale, J.A., 2003. Uranium-series chronology and environmental applications of speleothems. Rev. Mineral. Geochem. 52, 407–460. https://doi.org/10.2113/0520407.

Saha, S., Owen, L.A., Orr, E.N., Caffee, M.W., 2019. High-frequency Holocene glacier fluctuations in the Himalayan-Tibetan orogen. Quat. Sci. Rev. 220, 372–400. https://doi.org/10.1016/j.quascirev.2019.07.021.

Sandeep, N., Swapna, P., Krishnan, R., Farneti, R., Prajeesh, A.G., Ayantika, D.C., Manmeet, S., 2020. South Asian monsoon response to weakening of Atlantic meridional overturning circulation in a warming climate. Clim. Dynam. 54, 3507–3524. https://doi.org/10.1007/s00382-020-05180-y.

Sarr, A.-C., Husson, L., Sepulchre, P., Pastier, A.-M., Pedoja, K., Elliot, M., Arias-Ruiz, C., Solihuddin, T., Aribowo, S., Susilohadi, 2019. Subsiding Sundaland. Geology 47, 119–122. https://doi.org/10.1130/G45629.1.

Sathiamurthy, E., Voris, H.K., 2006. Maps of holocene sea level transgression and submerged lakes on the Sunda Shelf. Trop. Nat. Hist. 1–44.

Scholz, D., Hoffmann, D.L., 2011. StalAge - an algorithm designed for construction of speleothem age models. Quat. Geochronol. 6, 369–382. https://doi.org/10.1016/j.quageo.2011.02.002.

Seierstad, I.K., Abbott, P.M., Bigler, M., Blunier, T., Bourne, A.J., Brook, E., Buchardt, S. L., Buizert, C., Clausen, H.B., Cook, E., Dahl-Jensen, D., Davies, S.M., Guillevic, M., Johnsen, S.J., Pedersen, D.S., Popp, T.J., Rasmussen, S.O., Severinghaus, J.P., Svensson, A., Vinther, B.M., 2014. Consistently dated records from the Greenland GRIP, GISP2 and NGRIP ice cores for the past 104 ka reveal regional millennial-scale δ18O gradients with possible Heinrich event imprint. Quat. Sci. Rev., Dating, Synthesis, and Interpretation of Palaeoclimatic Records and Model-data Integration: advances of the INTIMATE project(INTegration of Ice core. Marine and TErrestrial records, COST Action ES0907) 106, 29–46. https://doi.org/10.1016/j.quascirev.2014.10.032.

Sirocko, F., Garbe-Schönberg, D., McIntyre, A., Molfino, B., 1996. Teleconnections between the subtropical monsoons and high-latitude climates during the last deglaciation. Science 272, 526–529. https://doi.org/10.1126/science.272.5261.526.

Steinke, S., Glatz, C., Mohtadi, M., Groeneveld, J., Li, Q., Jian, Z., 2011. Past dynamics of the East Asian monsoon: No inverse behaviour between the summer and winter monsoon during the Holocene. Global Planet. Change 78, 170–177. https://doi.org/10.1016/j.gloplacha.2011.06.006.

Steinke, S., Mohtadi, M., Prange, M., Varma, V., Pittauerova, D., Fischer, H.W., 2014. Mid- to Late-Holocene Australian–Indonesian summer monsoon variability. Quat. Sci. Rev. 93, 142–154. https://doi.org/10.1016/j.quascirev.2014.04.006.

Stott, L., Poulsen, C., Lund, S., Thunell, R., 2002. Super ENSO and global climate oscillations at millennial time scales. Science 297, 222–226. https://doi.org/10.1126/science.1071627.

Sun, Y., Clemens, S.C., Morrill, C., Lin, X., Wang, X., An, Z., 2012. Influence of Atlantic meridional overturning circulation on the East Asian winter monsoon. Nat. Geosci. 5, 46–49. https://doi.org/10.1038/ngeo1326.

Surakiatchai, P., Choowong, M., Charusiri, P., Charoentitirat, T., Chawchai, S., Pailoplee, S., Chabangborn, A., Phantuwongraj, S., Chutakositkanon, V., Kongsen, S., Nimnate, P., Bissen, R., 2018. Paleogeographic reconstruction and history of the sea level change at Sam Roi Yot National Park, Gulf of Thailand. Trop. Nat. Hist. 18, 112–134.

Tan, L., Shen, C.-C., Löwemark, L., Chawchai, S., Edwards, R.L., Cai, Y., Breitenbach, S.F. M., Cheng, H., Chou, Y.-C., Duerrast, H., Partin, J.W., Cai, W., Chabangborn, A., Gao, Y., Kwiecien, O., Wu, C.-C., Shi, Z., Hsu, H.-H., Wohlfarth, B., 2019. Rainfall variations in central Indo-Pacific over the past 2,700 y. Proc. Natl. Acad. Sci. USA 116, 17201–17206. https://doi.org/10.1073/pnas.1903167116.

Thompson, L.G., Severinghaus, J.P., Yao, T., Davis, M.E., Mosley-Thompson, E., Beaudon, E., Sierra-Hernández, M.R., Porter, S.E., 2022. Use of δ18Oatm in dating a Tibetan ice core record of Holocene/Late Glacial climate. Proc. Natl. Acad. Sci. USA 119, e2205545119. https://doi.org/10.1073/pnas.2205545119.

Tschudi, S., Schäfer, J.M., Zhao, Z., Wu, X., Ivy-Ochs, S., Kubik, P.W., Schlüchter, C., 2003. Glacial advances in Tibet during the younger Dryas? Evidence from cosmogenic 10Be, 26Al, and 21Ne. J. Asian Earth Sci. 22, 301–306. https://doi.org/10.1016/S1367-9120(03)00035-X.

University of East Anglia Climatic Research Unit, Harris, I.C., Jones, P.D., Osborn, T., 2022. CRU TS4.06: Climatic Research Unit (CRU) Time-Series (TS) Version 4.06 of High-Resolution Gridded Data of Month-By-Month Variation in Climate. Jan. 1901-Dec. 2021).

van Oldenborgh, G.J., 2020. KNMI Climate Explorer [WWW Document]. URL. https://climexp.knmi.nl/start.cgi. (Accessed 17 July 2020).

WAIS Divide Project Members, 2015. Precise interpolar phasing of abrupt climate change during the last ice age. Nature 520, 661–665. https://doi.org/10.1038/nature14401.

WAIS Divide Project Members, 2013. Onset of deglacial warming in West Antarctica driven by local orbital forcing. Nature 500, 440–444. https://doi.org/10.1038/nature12376.

Wang, B., LinHo, 2002. Rainy season of the asian–pacific summer monsoon. J. Clim. 15, 386–398. https://doi.org/10.1175/1520-0442(2002)015<0386:RSOTAP>2.0.CO, 2.

Wang, J.K., Johnson, K.R., Borsato, A., Amaya, D.J., Griffiths, M.L., Henderson, G.M., Frisia, S., Mason, A., 2019. Hydroclimatic variability in Southeast Asia over the past two millennia. Earth Planet Sci. Lett. 525, 115737 https://doi.org/10.1016/j.epsl.2019.115737.

Wang, X., Emerson, J.W., 2015. Bayesian Change Point Analysis of Linear Models on General Graphs. Pap, Work.

Wang, Y., Cheng, H., Edwards, R.L., He, Y., Kong, X., An, Z., Wu, J., Kelly, M.J., Dykoski, C.A., Li, X., 2005. The holocene Asian monsoon: links to solar changes and North Atlantic climate. Science 308, 854–857. https://doi.org/10.1126/SCIENCE.1106296.

Wang, Y.J., Cheng, H., Edwards, R.L., An, Z.S., Wu, J.Y., Shen, C.-C., Dorale, J.A., 2001. A high-resolution absolute-dated late Pleistocene monsoon record from Hulu cave, China. Science 294, 2345–2348. https://doi.org/10.1126/science.1064618.

Wassenburg, J.A., Vonhof, H.B., Cheng, H., Martínez-García, A., Ebner, P.-R., Li, X., Zhang, H., Sha, L., Tian, Y., Edwards, R.L., Fiebig, J., Haug, G.H., 2021. Penultimate deglaciation Asian monsoon response to North Atlantic circulation collapse. Nat. Geosci. 14, 937–941. https://doi.org/10.1038/s41561-021-00851-9.

Webster, P.J., Magaña, V.O., Palmer, T.N., Shukla, J., Tomas, R.A., Yanai, M., Yasunari, T., 1998. Monsoons: processes, predictability, and the prospects for prediction. J. Geophys. Res. Oceans 103, 14451–14510. https://doi.org/10.1029/97JC02719.

Wedepohl, K.H., 1995. The composition of the continental crust. Geochem. Cosmochim. Acta 59, 1217–1232. https://doi.org/10.1016/0016-7037(95)00038-2.

Wohlfarth, B., Klubseang, W., Inthongkaew, S., Fritz, S.C., Blaauw, M., Reimer, P.J., Chabangborn, A., Löwemark, L., Chawchai, S., 2012. Holocene environmental changes in northeast Thailand as reconstructed from a tropical wetland. Global Planet. Change 92 (93), 148–161. https://doi.org/10.1016/j.gloplacha.2012.05.008.

Wolf, A., Ersek, V., Braun, T., French, A.D., McGee, D., Bernasconi, S.M., Skiba, V., Griffiths, M.L., Johnson, K.R., Fohlmeister, J., Breitenbach, S.F.M., Pausata, F.S.R.,

Tabor, C.R., Longman, J., Roberts, W.H.G., Chandan, D., Peltier, W.R., Salzmann, U., Limbert, D., Trinh, H.Q., Trinh, A.D., 2023. Deciphering local and regional hydroclimate resolves contradicting evidence on the Asian monsoon evolution. Nat. Commun. 14, 5697. https://doi.org/10.1038/s41467-023-41373-9.

Wu, G., Liu, Y., He, B., Bao, Q., Duan, A., Jin, F.-F., 2012. Thermal controls on the asian summer monsoon. Sci. Rep. 2, 404. https://doi.org/10.1038/srep00404.

Wu, G., Liu, Y., Zhang, Q., Duan, A., Wang, T., Wan, R., Liu, X., Li, W., Wang, Z., Liang, X., 2007. The influence of mechanical and thermal forcing by the Tibetan plateau on asian climate. J. Hydrometeorol. 8, 770–789. https://doi.org/10.1175/JHM609.1.

Wurtzel, J.B., Abram, N.J., Lewis, S.C., Bajo, P., Hellstrom, J.C., Troitzsch, U., Heslop, D., 2018. Tropical Indo-Pacific hydroclimate response to North Atlantic forcing during the last deglaciation as recorded by a speleothem from Sumatra, Indonesia. Earth Planet Sci. Lett. 492, 264–278. https://doi.org/10.1016/j.epsl.2018.04.001.

Xu, C., Buckley, B.M., Wang, S.-Y.S., Pumijumnong, N., An, W., Sano, M., Nakatsuka, T., Guo, Z., 2019. Increased variability of Thailand's Chao Phraya river peak season flow and its association with ENSO variability: evidence from tree ring δ18O. Geophys. Res. Lett. 46, 4863–4872. https://doi.org/10.1029/2018GL081458.

Yamoah, K.A., Chabangborn, A., Chawchai, S., Fritz, S., Löwemark, L., Kaboth-Bahr, S., Reimer, P.J., Smittenberg, R.H., Wohlfarth, B., 2021. A muted El Niño-like condition during late MIS 3. Quat. Sci. Rev. 254, 106782 https://doi.org/10.1016/j.quascirev.2020.106782.

Yamoah, K.K.A., Chabangborn, A., Chawchai, S., Väliranta, M., Wohlfarth, B., Smittenberg, R.H., 2016. Large variability in n-alkane δ13C values in Lake Pa Kho (Thailand) driven by wetland wetness and aquatic productivity. Org. Geochem. 97, 53–60. https://doi.org/10.1016/j.orggeochem.2016.04.008.

Yan, C., Yao, J., Shen, X., Yang, H., 2023. Investigating the effect of the Tibetan Plateau on the ITCZ using a coupled Earth system model. Atmospheric Ocean. Sci. Lett. 16, 100294 https://doi.org/10.1016/j.aosl.2022.100294.

Yancheva, G., Nowaczyk, N.R., Mingram, J., Dulski, P., Schettler, G., Negendank, J.F.W., Liu, J., Sigman, D.M., Peterson, L.C., Haug, G.H., 2007. Influence of the intertropical convergence zone on the East Asian monsoon. Nature 445, 74–77. https://doi.org/10.1038/nature05431.

Yang, J., Li, G., Gan, Y., Chen, Z., Zhang, X., 2023. Role of the tropical Indian Ocean in orbitally induced mid-Holocene precipitation variation in northwest China. Quat. Sci. Rev. 317, 108285 https://doi.org/10.1016/j.quascirev.2023.108285.

Yang, Q., Scholz, D., Jochum, K.P., Hoffmann, D.L., Stoll, B., Weis, U., Schwager, B., Andreae, M.O., 2015. Lead isotope variability in speleothems—a promising new proxy for hydrological change? First results from a stalagmite from western Germany. Chem. Geol. 396, 143–151. https://doi.org/10.1016/j.chemgeo.2014.12.028.

Yang, X., Yang, H., Wang, B., Huang, L.-J., Shen, C.-C., Edwards, R.L., Cheng, H., 2019. Early-Holocene monsoon instability and climatic optimum recorded by Chinese stalagmites. Holocene 29, 1059–1067. https://doi.org/10.1177/0959683619831433.

Yuan, S., Chiang, H.-W., Liu, G., Bijaksana, S., He, S., Jiang, X., Imran, A.M., Wicaksono, S.A., Wang, X., 2023. The strength, position, and width changes of the intertropical convergence zone since the Last Glacial Maximum. Proc. Natl. Acad. Sci. USA 120, e2217064120. https://doi.org/10.1073/pnas.2217064120.

Zhang, H., Brahim, Y.A., Li, H., Zhao, J., Kathayat, G., Tian, Y., Baker, J., Wang, J., Zhang, F., Ning, Y., Edwards, R.L., Cheng, H., 2019. The asian summer monsoon: teleconnections and forcing mechanisms—a review from Chinese speleothem δ18o records. Quaternary 2. https://doi.org/10.3390/quat2030026.

Zhang, N., Yang, Y., Cheng, H., Zhao, J., Yang, X., Liang, S., Nie, X., Zhang, Y., Edwards, R.L., 2018. Timing and duration of the East Asian summer monsoon maximum during the Holocene based on stalagmite data from North China. Holocene 28, 1631–1641. https://doi.org/10.1177/0959683618782606.

Zhang, X., Knorr, G., Lohmann, G., Barker, S., 2017. Abrupt North Atlantic circulation changes in response to gradual CO2 forcing in a glacial climate state. Nat. Geosci. 10, 518–523. https://doi.org/10.1038/ngeo2974.

Zhu, Q., He, J., Wang, P., 1986. A study of circulation differences between East-Asian and Indian summer monsoons with their interaction. Adv. Atmos. Sci. 3, 466–477. https://doi.org/10.1007/BF02657936.